

TOPICAL REVIEW

Neutrino-driven wind simulations and nucleosynthesis of heavy elements

A. Arcones

Institut für Kernphysik, Technische Universität Darmstadt, Schlossgartenstraße 2,
D-64289 Darmstadt, Germany

GSI Helmholtzzentrum für Schwerionenforschung GmbH, Planckstr. 1 D-64291
Darmstadt, Germany

E-mail: almudena.arcones@physik.tu-darmstadt.de

F.-K. Thielemann

Department of Physics, University of Basel, Klingelbergstraße 82, 4056, Basel,
Switzerland

Abstract. Neutrino-driven winds, which follow core-collapse supernova explosions, present a fascinating nuclear astrophysics problem that requires understanding advanced astrophysics simulations, the properties of matter and neutrino interactions under extreme conditions, the structure and reactions of exotic nuclei, and comparisons against forefront astronomical observations. The neutrino-driven wind has attracted vast attention over the last 20 years as it was suggested to be a candidate for the astrophysics site where half of the heavy elements are produced via the r-process. In this review, we summarize our present understanding of neutrino-driven winds from the dynamical and nucleosynthesis perspectives. Rapid progress has been made during recent years in understanding the wind with improved simulations and better micro physics. The current status of the fields is that hydrodynamical simulations do not reach the extreme conditions necessary for the r-process and the proton or neutron richness of the wind remains to be investigated in more detail. However, nucleosynthesis studies and observations point already to neutrino-driven winds to explain the origin of lighter heavy elements, such as Sr, Y, Zr.

Submitted to: *J. Phys. G: Nucl. Phys.*

1. Introduction

Core-collapse supernovae contribute to the chemical enrichment of the interstellar medium (and thus to the next generation of stars) in two ways: they eject elements that were synthesized during the life of stars (e.g., helium, nitrogen, oxygen and carbon) and they produce new and heavier elements during the explosion. Although the link between core-collapse supernovae and the origin of heavy elements was done more than fifty years ago [1, 2], there have been many new and exciting developments in the field of supernovae nucleosynthesis. Here we want to summarize the nucleosynthesis in the neutrino-powered ejecta known as neutrino-driven wind of the newly born proto-neutron star.

The lightest elements were produced in the big bang, followed by the formation of the first stars and by the production of heavier elements in subsequent nuclear burning phases in their interiors. The death of the first stars enriches the interstellar medium, and the next generations of stars reprocess the previously expelled material. This process continues in recurrent star formation, stellar evolution, and stellar death stages (galactic chemical evolution). Although this synthesis is believed to be generally understood, key questions in the physics remain. For example, how do massive stars die in core-collapse supernova explosions? How are half of the elements heavier than iron produced?

Core-collapse supernovae mark the end of the life of stars with at least eight times the mass of our sun, leading to the birth of neutron stars and stellar-mass black holes. After millions of years of hydrostatic burning, no further energy can be gained from fusion and the iron core collapses when it reaches the maximum mass stabilized by the pressure of a degenerate electron gas. The collapse suddenly stops, when the core is compressed to nuclear densities by gravity, and the inner core bounces back, forming a shock wave. This supernova shock loses energy by photo-dissociation of iron-group nuclei in the material encountered by the passing shock wave. This leads to a stalled shock, and it remains an open question how it re-accelerates and produces a successful explosion (see Refs. [3, 4]). The best studied and still most promising mechanism to re-accelerate the shock is due neutrinos because they can transport the energy from the hot proto-neutron star to the shock.

After the successful launch of the supernova explosion, the proto-neutron star in the center cools by emitting neutrinos. The energy deposited by these neutrinos via capture and scattering events powers a baryonic outflow that expands with supersonic velocities and is known as the neutrino-driven wind. This neutrino-driven wind is a promising site for different nucleosynthesis processes and was proposed as the main host for the r-process. The general conditions required for the r-process can be studied using analytic [5] and steady-state [6, 7] models of neutrino-driven winds. These have established high entropy, fast expansion, and low electron fraction ($Y_e \approx 0.4$) as necessary to obtain a high ratio of neutrons to so-called seed nuclei in the iron group or beyond (neutron-to-seed ratio) which act as seeds for rapid neutron capture to form the heaviest elements. Parametric models show that a strong r-process can

occur [8, 9, 10], but only for conditions that are not reached in current long-time hydrodynamic simulations [11, 12, 13, 14].

At present it is unclear if the conditions in neutrino-driven winds are extreme enough for a successful r-process up to uranium, but it is certain that core-collapse supernovae are fascinating hosts where various nucleosynthesis processes produce neutron-rich and neutron-deficient nuclei. As suggested in Ref. [15], neutrino-driven winds can also be the site where lighter heavy elements (e.g., Sr, Y, Zr) are produced by the weak r-process or by the νp -process. These can account for the suggested lighter element primary process (LEPP) contribution [16], responsible for the abundances of these elements at low metallicities in very old stars where the s-process is not active yet.

1.1. Observational constraints

The fingerprints of supernova nucleosynthesis are observed in our solar system. The solar photosphere and meteorites reflect the chemical signature of the gas cloud where the Sun formed. These abundances show the combined results of different nucleosynthesis contributions and the imprints of nuclear physics. The fast decrease of the abundances towards the iron peak is due to the increasing Coulomb barrier for charged particle fusion reactions (with increasing proton number) that hinders the production of heavier elements. Then neutron capture takes over as main mechanism for forming heavier than iron-group nuclei, and one distinguishes between the s-process and r-process [1], which yield double peaks in the abundances corresponding to neutron magic numbers, $N = 50, 82, \text{ and } 126$.

The oldest stars observed, known as ultra metal-poor (UMP) stars, show lines of heavy elements in their spectra indicating that these elements were already expelled in very early r-process events [17]. These UMP stars are very rare, however their detection is increasing successful with large-scale surveys and new telescopes [18, 19] that are providing new insights in the origin of elements. When abundances of UMP stars are compared to the scaled solar system abundances, there are two clear underlying trends: 1) For elements between barium and lead ($56 < Z < 82$) the relative abundances are the same in UMP stars and in the r-process component of the solar system. This indicates that these elements are always produced in the same way by a *robust r-process*. This robustness can be due to the astrophysical scenario in combination with nuclear physics aspects. 2) The scatter for elements between strontium and silver ($38 < Z < 47$) indicates an additional contribution for the production of those *lighter heavy elements*. This contribution may be associated with a weak r-process (see Ref. [17] and references therein) involving charged-particle reactions [15].

The strong scatter of r-process contributions in comparison to regular supernova products like iron, measured e.g., by the Eu/Fe-ratio, seems to give an indication that strong r-process events are rare but efficient when they occur [20].

1.2. Structure of the review and definitions

This review is divided into two parts. First, we discuss the main features, parameters and nucleosynthesis of the neutrino-driven outflows (Sect. 2). The wind dynamics, which is key for determining the entropy and expansion time scale, are described in Sect. 2.1, while weak reactions and electron fraction uncertainties are introduced in Sect. 2.2. The role of these three wind parameters (entropy, expansion time scale, and electron fraction) on the nucleosynthesis is explained in Sect. 2.3. The possible additional ingredients that have been investigated are presented in Sect. 2.4. In the second part (Sect. 3), the different nucleosynthesis processes and their status based on recent supernova simulations are discussed. The developments of neutrino-driven wind models for studying the r-process are summarized in Sect. 3.1. The origin of lighter heavy elements (Sect. 3.2) can be explained by a weak r-process (Sect. 3.3) or by the νp -process (Sect. 3.4). Summary and outlook are in Sect. 4.

Before immersing us into the neutrino-driven wind, let's summarize a few useful concepts that will be used along the review.

Matter consisting of a composition of ionized nuclei can be described by the corresponding mass fractions X_i summing up to unity ($\sum_i X_i = 1$). A quantity which is not weighted with the total mass but rather proportional to the number density of a nucleus is the abundance $Y_i = X_i/A_i$. If the mass density of a nucleus ρX_i is divided by the mass of a nucleus $A_i m_u$, one obtains directly the number density $n_i = \rho X_i / (A_i m_u) = \rho Y_i / m_u = \rho N_A Y_i$, as $N_A = 1/m_u$ in the appropriate units. The total abundance of electrons (or also called electron fraction) is identical to the total abundance of protons (in free protons and nuclei) $Y_e = \sum_i Z_i Y_i$ and equivalent to the total proton-to-nucleon ratio $\sum_i Z_i Y_i / (\sum_i (Z_i + N_i) Y_i) = \sum_i Z_i Y_i / (\sum_i A_i Y_i) = \sum_i Z_i Y_i / (\sum_i X_i)$. Abundance changes (\dot{Y}_i) can be described by differential equations for each nuclear abundance Y_i , related to decays, fusion reactions and three body reactions (a sequence of two fusion reactions involving an intermediate particle-unstable nucleus, i.e. with a vanishing half-life), for details see Ref. [21]. Reactions with a (thermal or non-thermal) distribution of photons/neutrinos can be written like decay reactions (after integrating over the photon or neutrino energy spectra) with a decay “constant” having a temperature (or more complex) dependence.

2. Neutrino-driven outflows: features, parameters and nucleosynthesis

2.1. Wind dynamics: entropy and expansion time scale

When a massive star collapses at the end of its live, gravitational energy is transformed into internal energy. This leads to a hot proto-neutron star with initial temperatures of $kT \approx GMm_n/R \approx 30 - 50$ MeV. At this high temperature, neutrinos dominate the cooling and carry away the gravitational binding energy. Inside of the newly born neutron star, densities are very high and neutrinos are thus trapped. Neutrinos diffuse from the interior of the neutron star and can freely stream when their mean free path

becomes comparable to the neutron star radius. The region from where neutrinos escape, the *neutrinosphere*, is different for every flavor and energy as neutrino-matter interactions are strongly energy dependent. The *neutrinosphere* region is located at the outer layers of the proto-neutron star where density and temperature present steep gradients. Some of the escaping neutrinos deposit energy in the matter of this region mainly via charged-particle reactions:

$$\nu_e + n \rightarrow p + e^- \quad (1)$$

$$\bar{\nu}_e + p \rightarrow n + e^+ . \quad (2)$$

This injection of energy in the outer layers of the proto-neutron star causes that a significant fraction of mass of the outer neutron star layers is blown off in a *neutrino-driven wind*.

The neutrino-driven wind sets in after the explosion and lasts for several seconds and even minutes. This deleptonization eventually leads to a cold neutron star, transparent to neutrinos, and to a significant amount of matter being ejected during the first 10–20 s after the explosion. This initial cooling phase or neutrino-driven wind has been first described by Duncan et al. (1986) [22], a detailed study of the later cooling phase can be found in Ref. [23].

During the Kelvin-Helmholtz cooling time scale (i.e., the time it takes to radiate away the gravitational energy) the neutrino luminosities and energies and also the neutron star radius and mass change only slowly. Therefore, neutrino-driven winds can be assumed to be steady state outflows [22] described by the following equations:

$$\dot{M} = 4\pi r^2 \rho v \quad (3)$$

$$v \frac{dv}{dr} = -\frac{1}{\rho} \frac{dP}{dr} - \frac{GM}{r^2} \quad (4)$$

$$\dot{q} = v \left(\frac{d\epsilon}{dr} - \frac{P}{\rho^2} \frac{d\rho}{dr} \right) \quad (5)$$

for the mass, momentum, and energy conservation, respectively. Here \dot{M} is a constant mass outflow, ρ is the rest mass density, v is the outflow velocity, M is the mass of the neutron star, \dot{q} is the energy generation rate produced by neutrinos, and P and ϵ are pressure and specific energy that account for non-relativistic nucleons, relativistic electrons and positrons, and photon radiation [22, 5, 24]. There are two types of solutions for these equations with physical meaning. 1) For high mass outflows the velocity reaches the sound speed and shock region and neutron star are sonically disconnected. This is known as wind and it is schematically illustrated by the blue line in Fig. 1. 2) When the velocity does not attain the critical sound speed, we talk about a breeze solution (green lines, Fig. 1). Notice that there is only one physical supersonic or critical solution while one can find several subsonic or breeze solutions.

Steady state and analytic models have been developed to better understand neutrino-driven winds and their potential as r-process site, after the promising results of Woosley et al. (1994) [25]. Qian & Woosley (1996) [5] identified by means of an analytic model the wind parameters that are key for the nucleosynthesis of heavy elements.

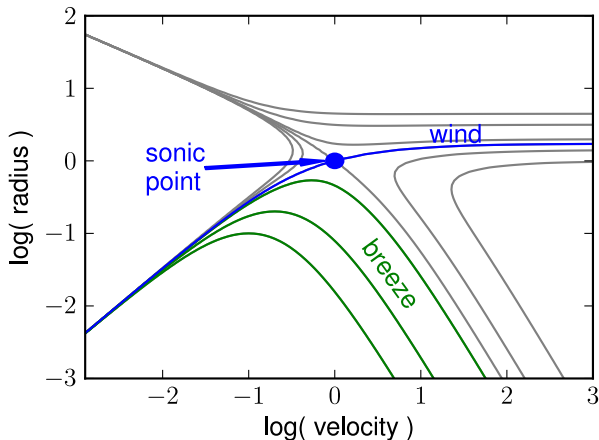


Figure 1. Schematic representation of the solutions of Eqs. (3)-(5). The blue line corresponds to the physical supersonic solution that crosses the sonic point. Some of the physical subsonic solutions are shown by the green lines and labeled as breeze. The grey lines represent mathematical solutions without physical meaning.

They assumed the wind to be a steady-state spherical outflow with boundaries at the neutrinosphere and supernova shock. Seconds after the explosion the shock is at large radii and there are only small and slow variations in the global neutrino characteristics and the properties of the neutron star. These support the steady-state assumption and permit to describe the wind independently of details how the shock gets launched. The impact of neutron star mass (M_{ns}) and radius (R_{ns}), and the neutrino luminosity (L_ν) and energy spectra (ϵ_ν) on the wind parameters can be understood with the following relations [5]:

$$\dot{M} \propto L_\nu^{5/3} \epsilon_\nu^{10/3} R_{ns}^{5/3} M_{ns}^{-2}, \quad (6)$$

$$s \propto L_\nu^{-1/6} \epsilon_\nu^{-1/3} R_{ns}^{-2/3} M_{ns}, \quad (7)$$

$$\tau \propto L_\nu^{-1} \epsilon_\nu^{-2} R_{ns} M_{ns}. \quad (8)$$

The mass outflow (\dot{M}) gives the amount of ejected mass and thus the contribution of neutrino-driven winds to the enrichment of heavy elements in the universe, provided the conditions in these mass zones support their nucleosynthesis. The wind entropy (s) and the expansion time scale (τ) are critical parameters to determine the composition of the ejecta.

The reactions responsible for the synthesis of heavy nuclei start at ^{12}C which is produced from ^4He via three body reactions (see Sect. 2.3). The efficiency of these reactions depends on the range of temperatures and densities. In a radiation-dominated environment the entropy is given by a relation including temperature and density: $S_w \propto T^3/\rho$. This is proportional to the photon-to-baryon ratio [26, 27]. At high entropies the temperature is also high for densities which permit three body reactions. High temperature causes photo-dissociation and prevents the formation of seed elements (Sect. 1.2). The expansion time scale also controls the efficiency of the three body reactions. If the expansion is very fast, alpha particles do not have sufficient time

to combine into seed nuclei. Therefore, entropy and expansion time scale are key to determine how alpha particles contribute to form seed nuclei.

2.2. Weak interactions: electron fraction

An additional wind parameter is the electron fraction which does not depend on the total neutrino luminosities and energies but on the relative contributions of neutrinos and antineutrinos to these quantities. In a neutrino-driven wind the two forward reactions in Eqs. (1) and (2) dominate and cause, e.g., the proton abundance time variation to be

$$\dot{Y}_p = -\lambda_{\bar{\nu}_e,p} Y_p + \lambda_{\nu_e,n} Y_n. \quad (9)$$

In case of a weak equilibrium, i.e., an equilibrium of production of neutrons and protons by these weak interaction reactions, we have $\dot{Y}_p = \dot{Y}_n = 0$. This gives a relation between Y_p and Y_n to be $Y_n/Y_p = \lambda_{\bar{\nu}_e,p}/\lambda_{\nu_e,n}$. On the other hand, the electron fraction Y_e (the electron to nucleon ratio, being in charge equilibrium equal to the proton to nucleon ratio),

$$Y_e = \frac{Y_p}{Y_p + Y_n} = \frac{1}{1 + \frac{Y_n}{Y_p}} \quad (10)$$

can be expressed as

$$Y_e = \frac{1}{1 + \frac{\lambda_{\bar{\nu}_e,p}}{\lambda_{\nu_e,n}}}. \quad (11)$$

Thus, for the the wind one can assume that the electron fraction is given by [5]:

$$Y_e \approx \left[1 + \frac{L_{\bar{\nu}_e}(\epsilon_{\bar{\nu}_e} - 2\Delta + 1.2\Delta^2/\epsilon_{\bar{\nu}_e})}{L_{\nu_e}(\epsilon_{\nu_e} + 2\Delta + 1.2\Delta^2/\epsilon_{\nu_e})} \right]^{-1} \quad (12)$$

where L_{ν_e} , ϵ_{ν_e} and $L_{\bar{\nu}_e}$, $\epsilon_{\bar{\nu}_e}$ are the electron neutrino and antineutrino luminosities and mean energies ($\epsilon_\nu = \langle \varepsilon^2 \rangle / \langle \varepsilon \rangle$), respectively. The neutron-proton mass difference is $\Delta = m_n - m_p = 1.293$ MeV. In order to have a neutron-rich wind, i.e., $Y_e < 0.5$, the neutrino and antineutrino energies have to approximately fulfill $\epsilon_{\bar{\nu}_e} - \epsilon_{\nu_e} \gtrsim 4\Delta \approx 5$ MeV. Indeed, this is not found in recent spherically symmetric simulations [13, 12] where the neutrino outflow stays proton-rich. Under such conditions the rapid neutron capture process to form the heaviest nuclei cannot occur, ruling out the spherically symmetric neutrino-driven winds as its astrophysical site. However, this conditions become very favourable for the νp -process [28].

Here we would like to shortly summarize the historical evolution of research efforts for the wind electron fraction. Improvements in the neutrino reactions have resulted in a reduction of the electron antineutrino energy from the first simulations by Wilson to the modern ones [13, 12]. Moreover, all neutrino flavours have very similar energies which leads to proton-rich conditions since the requirement $\epsilon_{\bar{\nu}_e} - \epsilon_{\nu_e} \gtrsim 4\Delta \approx 5$ MeV is not fulfilled. This is illustrated in the neutrino two-color plot presented in Fig. 2. The question about the apparent proton-richness in neutrino-driven winds can then be reformulated: why are neutrino energies similar for all neutrino flavours?

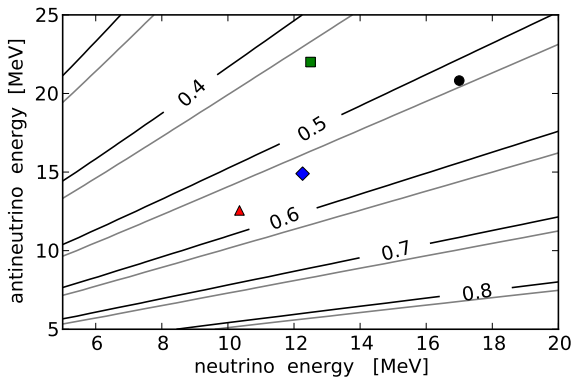


Figure 2. Estimated electron fraction (Eq. (12)) for different supernova models. The symbols show the electron neutrino and antineutrino energies ($\epsilon_{\nu_e} \approx 4.1kT_{\nu_e}$): square for Ref. [25], circle for model M15-11-r6 of Ref. [11], triangle for a $10 M_{\odot}$ progenitor of Ref. [12], and diamond for Ref. [13], all at 10 s after bounce. The black contours correspond to $L_{\bar{\nu}_e}/L_{\nu_e} = 1$ and the grey contours to $L_{\bar{\nu}_e}/L_{\nu_e} = 1.1$.

Neutrino energies depend on the temperature of the medium in the region where neutrinos decouple from matter. This region is known as the *neutrinosphere* and its location is different for each neutrino flavor and energy. Inside of the *neutrinosphere*, neutrinos are in thermal and chemical equilibrium mainly through charged-current reactions (Eqs. (1)-(2)). Outside the *neutrinosphere*, neutrinos escape and their temperature stays almost constant and approximately equal to the temperature at their *neutrinosphere*. Because neutrons are more abundant than protons in the neutron star, electron neutrinos continue interacting up to larger radii and thus to lower temperatures than antineutrinos ($\epsilon_{\bar{\nu}_e} \gtrsim \epsilon_{\nu_e}$). The muon and tau (anti)neutrinos interact only via neutral-current reactions and decouple at smaller radii, therefore their energies are larger. During the first seconds after the explosion, the proto-neutron star deleptonizes and the amount of protons in the outer layers decreases. The electron antineutrino energies are thus expected to be higher than the electron neutrino energies. However, this simple picture is not valid and the spectra of electron neutrinos and antineutrinos are rather similar due to neutral-current reactions that act in a similar way on all neutrino flavors and become also important as the neutron star cools [13, 29, 30, 31].

Moreover, the latest investigations of charged-current neutrino opacity [32, 33, 34] indicate that these cross sections can significantly change due to in medium modifications [35]. In the early supernova explosion phase, mean field effects have a minor effect on the neutrino spectra because *neutrinospheres* are not at very high densities. In the region where mean field effects are relevant neutrinos are trapped. In contrast, during the neutrino-driven wind phase, *neutrinospheres* are at high densities ($\rho \approx 10^{12} \text{gcm}^{-3}$) and mean field effects are not negligible although they are not included in current supernova simulations [13, 12]. As suggested in Refs. [32, 33, 34], the consideration of in medium modifications could change the electron fraction towards more neutron-rich conditions ($Y_e \approx 0.45$). However, the exact Y_e value depends on medium correlations and the

equation of state, both of which are still uncertain. In any case, these new results rise an exciting possibility of linking the wind nucleosynthesis to the behaviour of matter and neutrinos under extreme conditions in the proto-neutron star.

In addition, neutrino oscillations (see Sect. 2.4 for more details) and the presence of light clusters such as ${}^2\text{H}$, ${}^3\text{H}$, ${}^3\text{He}$ [29] also may change the electron fraction of the wind.

2.3. Nucleosynthesis and wind parameters

A mass element is ejected from the outer layers of the proto neutron star due to the energy deposited by neutrino. The nucleosynthesis in neutrino-driven winds starts at high temperatures and densities which keep the matter in nuclear statistical equilibrium (NSE), i.e., there is a balance (i.e., chemical equilibrium) between nuclear reactions producing seed nuclei (Z, A) and photo-dissociation destroying those nuclei into nucleons:



This leads to a relation between the chemical potentials, $\mu_{(Z,A)} = (A - Z)\mu_n + Z\mu_p$. Therefore, the composition can be calculated utilizing Boltzmann distributions for nuclei, neutrons, and protons. The composition is thus uniquely determined by the temperature, density, and electron fraction, being environment parameters:

$$Y(Z, A) = G_{Z,A}(\rho N_A)^{A-1} \frac{A^{3/2}}{2^A} \left(\frac{2\pi\hbar}{m_u kT} \right)^{\frac{3}{2}(A-1)} \exp(B_{Z,A}/kT) Y_n^{A-Z} Y_p^Z \quad (14)$$

where $G_{Z,A}$ is the nuclear partition function, $B_{Z,A}$ is the binding energy, \hbar is the Planck constant, N_A is the Avogadro number, and ρ is the baryon density. Equation (14) indicates that the presence of a nucleus depends strongly on kT , $B(Z, A)/kT$, and A . For moderate temperatures iron-group nuclei are favored in NSE because of their large binding energies. In contrast, at high temperatures many energetic photons are available, and the result is a gas consisting mostly of nucleons and alpha particles in which it is difficult to build up heavy nuclei because they are quickly photo-dissociated (see Ref. [27]). Very high densities would favor in contrast very heavy nuclei.

The NSE composition at high temperatures is dominated by alpha particles and nucleons. Only when the temperature drops, the alpha particles recombine and form seed nuclei at expenses of nucleons whose abundances drop rapidly. As the expansion continues and matter cools, slower reactions fall out of equilibrium. At the breakdown of NSE ($T \sim 8 - 5 \cdot 10^9$ K) for low densities, as occurring in the neutrino wind, the composition is dominated by alpha particles and one talks about alpha-rich freeze out. Alpha particles combine into seed nuclei starting with the triple-alpha reaction ($3\alpha \rightarrow {}^{12}\text{C}$). If the amount of free neutrons is not negligible, ${}^{12}\text{C}$ forms also via ${}^4\text{He}(\alpha n, \gamma) {}^9\text{Be}(\alpha, n) {}^{12}\text{C}$ [36]. These reactions depend strongly on the density and can be hindered if the expansion is very fast, i.e., if the density does not stay for sufficiently long time in the range where these three body reactions are effective ($\rho \sim 5 \cdot 10^6 \text{gcm}^{-3}$). The

production of ^{12}C is followed by the alpha process [36, 37] which consist of a sequence of alpha captures (including (α, γ) , (α, n) , and (α, p) reactions) combined with (n, γ) and (p, γ) reactions depending on the neutron-richness of the wind. These charged-particle reactions (CPR) continue until temperatures are too low to overcome the Coulomb barrier of nuclei ($T \sim 10^9$ K). The composition at CPR freeze-out consists mainly of alpha particles together with a few seed nuclei (formed by the alpha-process) and free nucleons. The proton or neutron richness as well as the ratio of nucleons and seed nuclei depends on the wind parameters and will determine the nucleosynthesis processes taking place in neutrino-driven winds. For example, the r-process can build heavy elements up to Uranium if the neutron-to-seed ratio (Y_n/Y_{seed}) is sufficiently high. Assuming the average mass number of seed nuclei is \bar{A}_{seed} , the neutron-to-seed indicates the heaviest elements (with mass number $\sim A$) that can be synthesized: $Y_n/Y_{\text{seed}} + \bar{A}_{\text{seed}} \sim A$. These two key quantities, \bar{A}_{seed} and Y_n/Y_{seed} , depend on the electron fraction, entropy, and expansion time scale [36, 8]. Freiburghaus et al. (1999) [9] analyzed in a site independent, entropy based approach abundance features and the impact of nuclear physics with especial focus on the dynamical evolution up to the freeze-out of final neutron captures in the r-process.

In order to understand better the evolution of the composition and its dependency on wind parameters during and after NSE we present in Figure 3 an overview based on the parametric trajectories described in Appendix A. Different columns represent various wind entropies and the rows correspond to various expansion time scales. For every combination of entropy and time scale the impact of the electron fraction is also shown by different color lines. These figures cover the evolution from NSE over charged-particle freeze-out to the weak or strong r-process. When the alpha abundances (dotted lines) become constant, the charged-particle reactions freeze out. At this moment one can get the neutron-to-seed ratio from the abundances of neutrons (solid lines) and nuclei (dashed lines). Note that after a few seconds the nuclei (dashed lines) are not seed nuclei anymore but the product of further neutron capture reactions. The impact of the wind parameters can be summarize based on Figure 3:

- At high entropies photo-dissociation prevents the formation of seed nuclei, therefore the abundance of neutrons stays higher for longer times. This behaviour is apparent from the right column of the panels with fast expansion. These evolutions will allow for a strong r-process. The impact of the wind entropy have been broadly discussed in the literature (see e.g., [27, 9, 8]).
- Fast expansion hinders the three body reactions which mark the beginning of the seed nuclei formation. During the production of seed nuclei neutrons are used to form alpha particles and heavy nuclei. Therefore, a fast expansion increases the neutron-to-seed ratio and favours the r-process.
- The electron fraction directly determined the amount of neutrons and protons. Lower Y_e leads to higher Y_n and lower Y_p . Notice that for $Y_e = 0.49$ the behavior of seed nuclei and neutrons is not always straight forward, see panel for

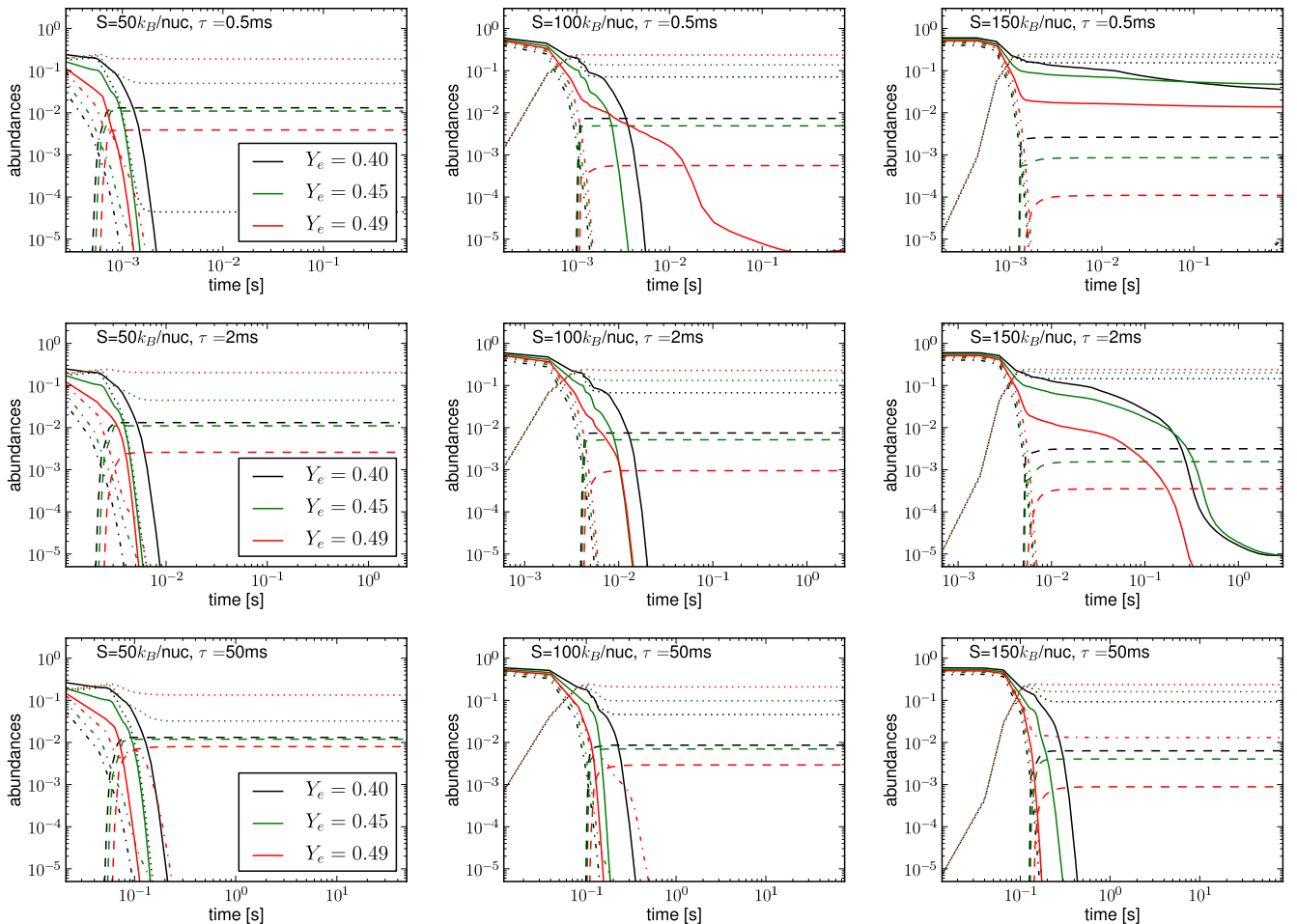


Figure 3. Evolution of abundances of neutrons (solid line), protons (dashed-dotted line), alpha particles (dotted line), and heavier nuclei (dashed line) for different electron fractions as indicated by the colors in the caption. The columns correspond to different entropies: $S = 50, 100, 150 k_B/\text{nuc}$ from the left to the right. The three rows are based on expansions with various time scales, as indicated in the panels, $\tau = 0.5, 2, 50$ ms.

$S = 100 k_B/\text{nuc}$ and $\tau = 0.5$ ms. A similar trend was seen in Ref. [8].

Figure 4 shows abundances corresponding to the different panels of Figure 3. This allows to link the wind parameters, which determine the neutron-to-seed ratio, to the elemental abundances and thus to the nucleosynthesis processes. For a high entropy ($S > 150 k_B/\text{nuc}$) and fast expansion ($\tau < 2$ ms) the r-process can form heavy elements. The other less extreme cases produce elements up to different proton numbers. For electron fraction close to 0.5 and a slow expansion with low entropy, the abundances result from charged particle reactions. For intermediate cases one talks about a weak r-process which reaches $N = 50$ (see Sect. 3.3). The last possibility, which is not presented here but will be discussed later, is the νp -process which builds heavy elements on the proton-rich side under high neutrino fluxes (Sect. 3.4).

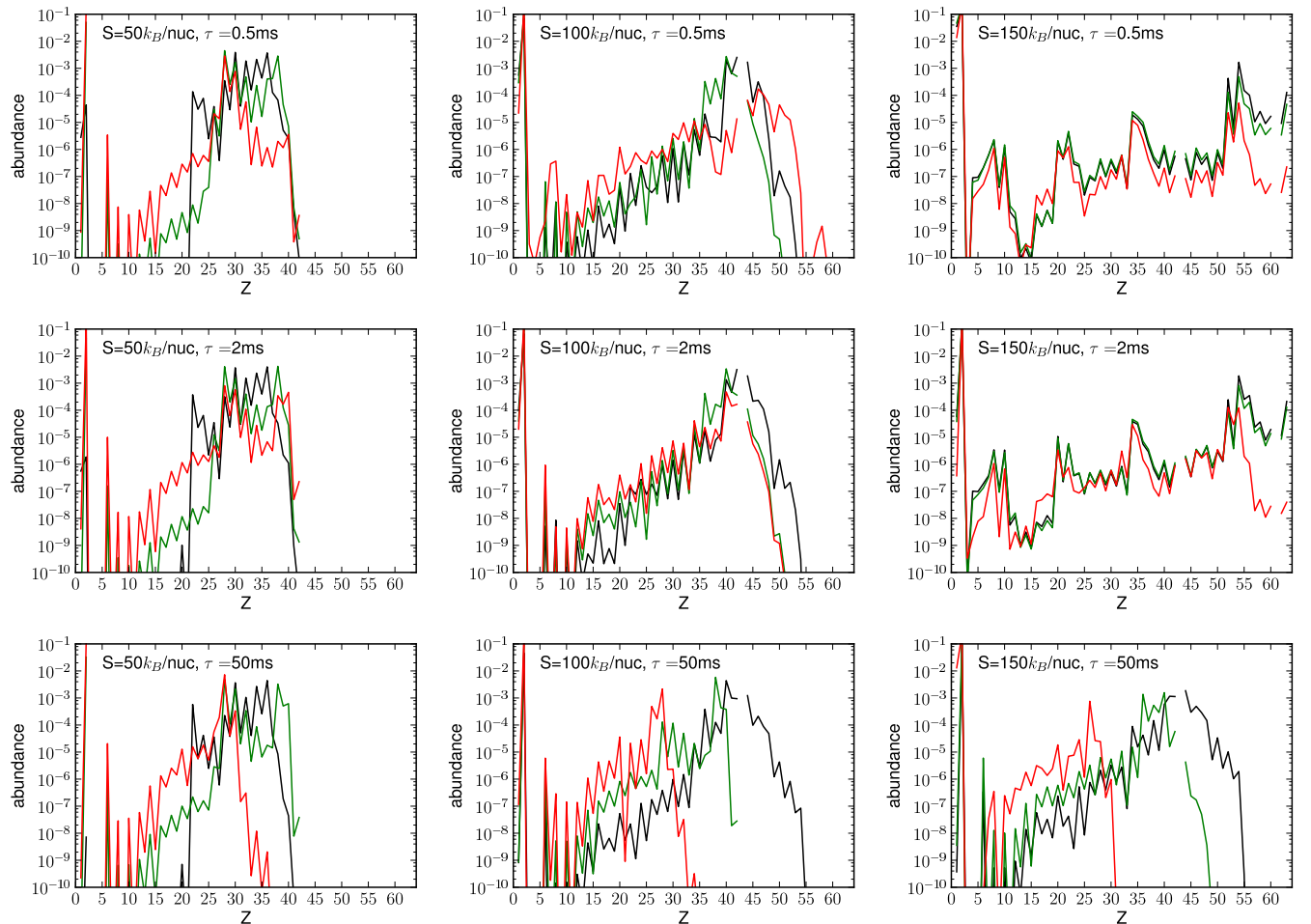


Figure 4. Elemental abundances for different electron fractions: $Y_e = 0.40$ (black), 0.45 (green), 0.49 (red). The entropy and expansion time scale are given in the figures and are distributed as in Figure 3.

2.4. Additional ingredients

The evolution of neutrino-driven winds is more complicated than the simplified description of the previous section. The wind parameters can become time-dependent due to an outer boundary, extra energy sources, rotation and magnetic fields, or neutrino oscillations. There have been several attempts of finding missing physical ingredients which could lead to either an entropy increase, a shorter expansion time scale, or reduction of the electron fraction. We discuss in this section, the main additional ingredients that have been explored with the goal of obtaining the r-process in neutrino-driven winds.

Wind termination

The neutrino-driven wind expands through the early, slow expanding supernova ejecta. When the wind becomes supersonic and the early ejecta move slowly, the collision of

both results in a wind termination shock or reverse shock. This hydrodynamical feature has been found in several supernova simulations [38, 39, 40, 11, 41, 12]. Qian & Woosley (1996) [5] first used in a steady state model an outer boundary with constant pressure at a radius corresponding to a temperature of ≈ 2 GK. The outcome was a slight increase of the entropy and a reduction of the expansion time scale. In supersonic wind models [7] an outer boundary is necessary to decelerate the wind. In contrast in subsonic winds or “breeze” [6, 42], the wind velocity naturally decreases (see Sect. 2.1). Other nucleosynthesis studies of the wind termination also imposed an outer boundary pressure [43] or kept the temperature constant [44].

The neutrino-driven wind was studied in detail for the first time by means of modern, high-resolution, long-time hydrodynamical simulations in Ref. [11]. Unlike the steady-state models, where the wind expands freely, in reality the wind moves through the early supernova ejecta. The interaction of the wind with the slow ejecta is not a steady-state phenomenon, therefore hydrodynamical simulations are required to study it in a consistent way. The evolution of the wind termination shock or reverse shock was investigated in Ref. [11] for different stellar progenitors and various evolutions of the inner boundary (i.e., contraction and compactness of the neutron star and neutrino luminosity evolution). It was found that the reverse shock radius (R_{rs}) depends on the wind mass outflow (\dot{M}) and velocity (v_w), but also on the pressure of the slow, early supernova ejecta:

$$R_{rs} \propto \sqrt{\frac{\dot{M}v_w}{P_{rs}}}. \quad (15)$$

The pressure in the supernova ejecta (P_{rs}) is linked to the explosion energy (E_{exp}) and to the progenitor, through the shock radius (R_s) with: $P_{rs} \propto E_{\text{exp}}/R_s^3$. Moreover, convection and anisotropies have a strong impact on this pressure and thus on the reverse shock radius [41]. When the supersonic neutrino wind collides with the early supernova ejecta, the kinetic energy is transformed into internal energy. The density and temperature of the shocked matter are thus higher than in the wind (see Fig. 6). The entropy at the reverse shock also increases and can be estimated as [11]:

$$s_{rs} \approx \left[\frac{s_w^{4/3}}{\beta^{1/3}} + 28.7 \frac{R_{rs,8}^{2/3} v_{s,9}^{7/2}}{\dot{M}_{-5}^{1/3}} \right]^{3/4}. \quad (16)$$

Here β is the relative jump in density at the reverse shock, $R_{rs,8}$ the reverse shock radius in units of 10^8 cm, $v_{w,9}$ the wind velocity in units of 10^9cm s^{-1} , and \dot{M}_{-5} the mass outflow normalized to $10^{-5} M_\odot$. If the wind entropy (s_w) is much smaller than the entropy at the reverse shock (s_{rs}), only the second term is relevant. For a $10 M_\odot$ progenitor, the entropy of the shocked matter can rise above $400 k_B/\text{nuc}$ [11]. For this low mass progenitor the ram pressure is very small and the supernova shock front expands very fast reaching large radii. This leads to a reduction of the pressure in the early supernova ejecta (P_{rs}) and to an increase of the reverse shock radius (Eq. 15). This and the larger wind velocity for this progenitor contribute to obtaining high entropies at the

position of the reverse shock (Eq. 16). However, this high entropy is attained only when the temperature is already relatively low, $T_{rs} \approx 2 - 0.4$ GK. For a successful r-process in neutrino-driven winds, the entropy has to be high when the neutron-to-seed ratio is established. This occurs at high temperature when charged-particle reactions are still building seed nuclei at expenses of neutrons.

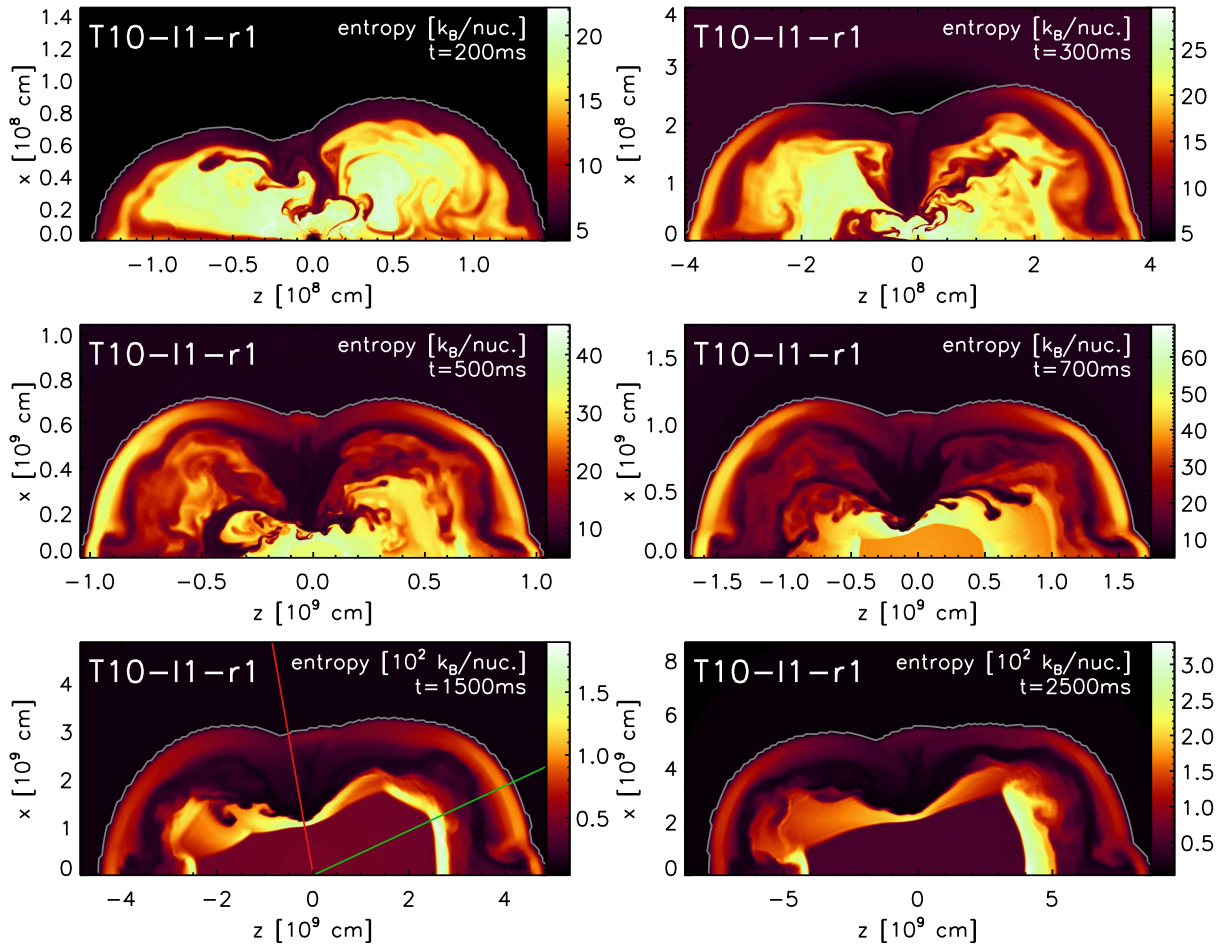


Figure 5. Entropy distribution in model T10-l1-r1 [41] for different times after bounce as indicated in every panel. The thin grey line marks the shock radius. In the panel for $t = 1500$ ms, the radial lines mark the angular directions at $\theta = 25$ degrees (green line) and 100 degrees (red line), along which radial profiles are shown in Fig. 6.

Multidimensional simulations [41] indicate that the wind stays spherically symmetric also in two-dimensional simulations. This is expected as the neutrino emission from the spherical neutrinosphere is isotropic in absence of rotation. However, the anisotropic pressure distribution of the early ejecta has a big impact on the position of the reverse shock and thus on the long-time evolution. Figure 6 shows the entropy distribution at different times after bounce. The central region with constant entropy (appearing at 700 ms) is the neutrino driven wind. Note the very anisotropic form of the wind termination. The expansion after the wind phase can be very different, therefore,

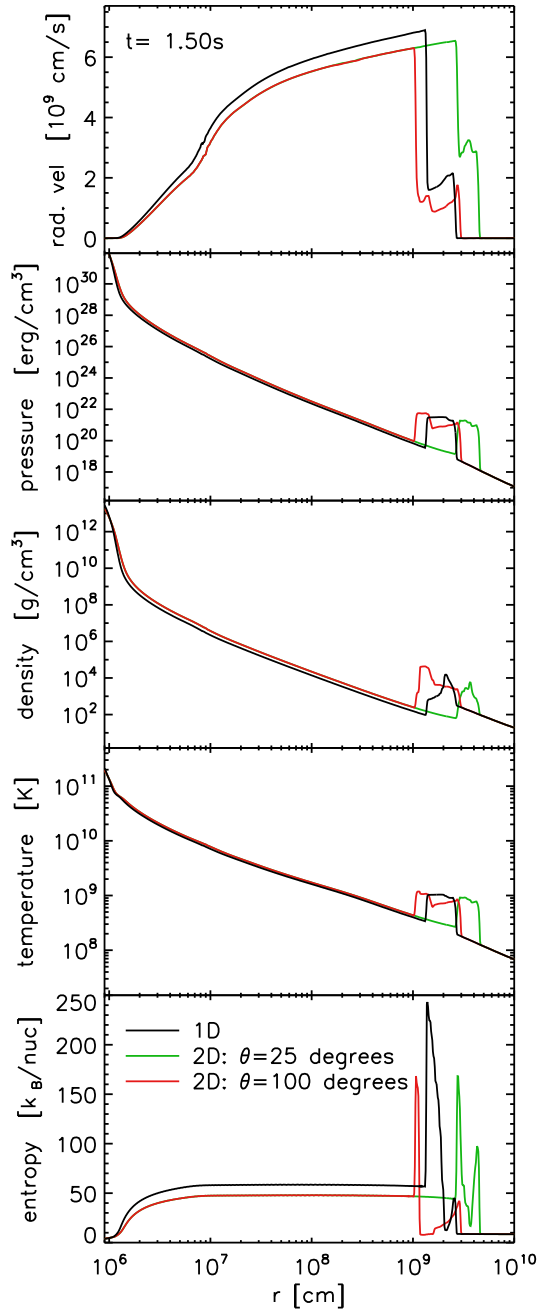


Figure 6. Comparison of one (black lines) and two-dimensional wind simulations showing the profiles of radial velocity, pressure, density, temperature, and entropy as functions of radius at time 1.5 s after bounce. The one-dimensional model correspond to M10-l1-r1 described in Ref. [11]. For the two-dimensional model T10-l1-r1 [41], the profiles are shown at angles $\theta = 25$ degrees (green lines) and $\theta = 100$ degrees (red lines), corresponding to the lines of the same colors in Fig. 5 (panel for $t = 1500$ ms).

if one uses parametric wind models, it is recommended to vary the extrapolation (see Appendix B).

Different groups [45, 46, 47] have studied the impact of the reverse shock assuming

the r-process does occur in neutrino-driven winds. In addition, the wind termination can also affect the νp -process ([48, 49], Sect. 3.4).

Extra energy source

An extra energy source can lead to an increase of the wind entropy. Qian & Woosley (1996) [5] explored this possibility by artificially increasing the energy at different positions. If the artificial energy source is close to the neutron star, most of the energy goes into work against gravity without a significant increase of entropy. If energy is deposited far out, in regions where the temperature has dropped to 2 GK, then there may be an impact on the r-process. If the extra energy source affects the region where the mass outflow is determined ($\sim 15\text{--}35$ km), then the entropy increases and the expansion time scale drops. Both together are sufficient to have a successful r-process. The problem is to identify such energy source. Qian & Woosley (1996) [5] checked the uncertainties in neutrino interactions and concluded that those are not sufficient to account for the extra energy required. Wanaajo (2006) [50] showed that extra energy could be the outcome of an anisotropic neutrino emission. Assuming a hot spot in the neutron star that emits more neutrinos and using a simple model, r-process favourable conditions were found. However, the origin of such a big anisotropy is not yet clear. Further investigations based on multidimensional simulations are necessary to understand this possibility better.

Rotation and magnetic fields

Rotation and magnetic fields have been also included in steady-state winds [51, 52, 53, 54]. Thompson (2003) [52] studied the effect of strong dipole magnetic fields and showed that matter is initially trapped by close field lines. Later this matter escapes dynamically due to neutrino heating and gets higher pressure and entropy, although the expansion is slightly slower. For neutron-rich conditions ($Y_e < 0.5$) and magnetic fields of $B \gtrsim 10^{14}$ G the entropy increases sufficiently to reach r-process favourable conditions. The amount of matter ejected in these magnetic winds is higher ($\dot{M} \sim 10^{-4} M_\odot$) than in standard winds without magnetic fields. However, these events are much too infrequent, in order to fulfill galactic chemical evolution constraints. Suzuki & Nagataki (2005) [53] showed that Alfvén waves in strong magnetized neutron stars [55] can accelerate the wind and deposit energy. These waves can thus account for the extra energy source suggested by Qian & Woosley (1996) [5] when the magnetic field reaches $B \approx 3\text{--}5 \cdot 10^{14}$ G. Moreover, Metzger et al. (2007) [54] solved the magneto hydrodynamic (MHD) wind equations for different rotation periods and magnetic fields. With dipole fields of $B^{\text{dip}} \gtrsim 10^{15}$ G and rotation periods of $P \approx 10$ ms they were able to get closer to the limiting conditions for a successful r-process [8]. Although strong magnetic field and fast rotation are not enough to produce r-process nuclei, MHD waves can lead to sufficient energy to increase the entropy in agreement with Ref. [53].

Neutrino oscillations

All the additional ingredients discussed above bring the neutrino-driven wind closer to

a successful r-process but only if the wind is neutron rich, i.e., $Y_e < 0.5$. As explained in Sect. 2.2, there are still uncertainties on the determination of Y_e . The r-process cannot occur in spherical neutrino-driven winds unless it becomes sufficiently neutron rich. One possibility to alter the electron fraction are neutrino oscillations. These can increase the energy of electron antineutrinos or/and reduce the electron neutrino fluxes. For the first to occur, energetic neutrinos (ν_τ , ν_μ) need to oscillate into electron neutrinos. This could occur via collective neutrino oscillations [56]. However, the neutrino spectra become very similar for all neutrino flavours during the wind phase [13] and thus no big increase of the electron antineutrino energies is expected in this way. Notice that this high energy could be important in proton-rich conditions for the νp -process [57]. Another exciting possibility is due to matter-enhanced active-sterile oscillations as it was suggested in Ref. [58]. The existence of sterile neutrinos remains an open question and it has been used to explain anomalies in some detector experiments [59]. This oscillation reduces the electron neutrino flux at relative large radii, where the effective neutrino heating has already occurred. McLaughlin et al. (1999) [58] showed that with the right combination of neutrino parameters, electron neutrinos oscillate into sterile neutrinos when $Y_e > 0.3$, while when $Y_e < 0.3$ antineutrinos are the ones that oscillate. Similar discussions with sterile neutrinos can be found in Refs. [60, 61, 62]. Recently, a systematic study has been performed [63] based on a low mass supernova progenitor. They found sterile neutrinos could mix with active states and strongly impact Y_e . They considered also collective active-active oscillations which become more significant at later times and shift Y_e towards higher values. Although there is no clear proof of the existence of sterile neutrinos, there is still room to explore the impact of this exotic phenomenon for the neutrino-driven wind nucleosynthesis.

3. Nucleosynthesis in neutrino-driven winds

The nucleosynthesis processes that can occur in neutrino-driven winds depend on the wind parameters. If the electron fraction is below 0.5, there are two possibilities depending on the neutron-to-seed ratio. High entropies and fast expansions lead to high $Y_n/Y_{\text{seed}} \gtrsim 100$ which allows the r-process to build heavy elements up to uranium. When the conditions are less neutron rich and the neutron-to-seed ratio is low ($Y_n/Y_{\text{seed}} \lesssim 1$), elements up to $N = 50$ are synthesized in a weak r-process. Proton-rich winds are another possibility which is favoured by current supernova models. In this case the νp -process can produce elements heavier than ^{64}Ge along proton rich nuclei. The weak r-process and the νp -process make neutrino-driven winds an exciting scenario to explain the origin of lighter heavier elements such as Sr, Y, and Zr.

3.1. r-process

The extreme conditions required for the r-process are not found in spherically symmetric neutrino-driven winds. However, high entropy winds have been the center of many

nucleosynthesis studies based on steady state, parametric and hydrodynamic models. Here we summarize the historical developments of the r-process in neutrino-driven winds. Past investigations were also dedicated to analyze key aspect for the r-process, e.g., nuclear physics input and impact of the dynamical evolutions. These studies are critical to understand the r-process in general for any astrophysical scenario.

3.1.1. Historical overview: In the 90’s a new era started for the nucleosynthesis in core-collapse supernovae and the developments of neutrino-driven wind studies. Since 1957 core-collapse supernovae have attracted interest as the astrophysical site where heavy elements are synthesized by the r-process [1, 2]. First nucleosynthesis studies based on simple hydrodynamical simulations were performed already by Hillebrandt et al. (1976) [64]. These relied on prompt supernova explosions where neutron rich matter from the outer layers of the proto-neutron star is hydrodynamically ejected. Although the solar system abundances could be approximately reproduced, the amount of r-process material ejected in such events leads to an overproduction of heavy elements if all core-collapse supernovae had exploded in this way [65]. The total mass fraction of r-process material in our galaxy accounts for $\sim 10^4 M_\odot$ of the total $\sim 10^{11} M_\odot$. As the supernova rate is $\sim 10^{-2} \text{yr}^{-1}$ [66] and the age of the galaxy when the solar system formed was 10^{10}yr , the r-process material produced per supernova in the history of the galaxy can be only $\lesssim 10^{-4} M_\odot$, assuming the r-process takes place in every supernovae. Therefore, Hillebrandt et al. (1976) [64] argued that the prompt explosions rich in r-process material are rare events. By now we know that the prompt shock bounce after the collapse is not sufficient to lead to a successful supernova explosion but occurs by some delayed mechanism [67, 68, 69, 12].

First delayed neutrino-driven explosions were reported by Bethe & Wilson (1985) [70] and followed by many nucleosynthesis studies. Two groups studied the late hydrodynamical evolution based on Wilson explosions.

Woosley & Hoffman (1992) [36] studied the nucleosynthesis from NSE to the alpha-rich freeze-out of charged particle reactions in the high entropy wind from the nascent proto-neutron star. They suggested that the later evolution could lead to high entropy and low electron fractions and thus to a successful r-process. In a following paper, Meyer et al. (1992) [26] followed the evolution and nucleosynthesis after the alpha-rich freeze-out based on different values of Y_e . The final abundances, based on a superposition of various trajectories with different neutron excess, agreed rather well with the solar system abundances. Finally, Woosley et al. (1994) [25] performed hydrodynamical simulations with the spherically symmetric radiation hydrodynamic code of Wilson & Mayle (1993) [71] for a $20 M_\odot$ progenitor and followed the evolution of the ejecta for 20 s after the explosion. Already 5 s after bounce appropriate conditions for the r-process were found in the $10^{-4} M_\odot$ ejected by the wind. A nice agreement with solar system r-process abundances was obtained only with a small overproduction around $A = 90$. The success of this work was summarized at the end of their paper: “... the problem is in need of further study, but we are gratified to have found what seems to be the most

promising site yet proposed for the production of the r-process elements”.

However, already in the same year these results could not be reproduced by an independent group. Wittl et al. (1994) [37] used also a Wilson supernova model for a $25M_{\odot}$ star and studied the late evolution starting at 0.6 s after bounce. They found entropy values below $100 k_B \text{nuc}^{-1}$ and electron fractions above 0.45, compared to $S \sim 400 k_B \text{nuc}^{-1}$ and $Y_e \sim 0.35$ reported by Woosley et al. (1994) [25]. In their first paper [37], the moderate entropy of their models resulted in an alpha-rich freeze-out with too many seed nuclei and too few neutrons. This led, similar to Ref. [36], to a strong overproduction of nuclei around $A = 90$, related to the neutron magic number $N = 50$. Their second paper [72] presents the possibility of having an r-process in the neutrino-driven winds if the entropy is assumed to be larger. Increasing the entropy by a factor 5.5 (reducing the density by the same factor, $S \propto T^3/\rho$) reproduced the solar system abundances and solved the overproduction problem for $A \sim 90$. They concluded that “the neutrino wind in core-collapse supernovae is a very promising site for the r-process nucleosynthesis”, but still “much remains to be worked out”.

These both works presented the exciting possibilities for the r-process in neutrino-driven winds and identified the three key parameters: entropy, expansion time scale, and electron fraction. However, the results did not agree and were far from being final. Further detailed studies of the wind and supernovae were necessary and have emerged since then.

Qian & Woosley (1996) [5] studied the wind based on an analytic model and could not find appropriate conditions for an r-process in general, therefore investigated the impact of missing ingredients, such as an outer boundary or an extra energy source (see Sect. 2.4). They concluded that any effect that strengthens the gravitational potential leads to an increase of the entropy. Following this line, Cardall & Fuller (1997) [73] included a general relativity treatment of the wind. The outcome of this study was a more compact neutron star and, consequently, higher wind entropy than in the Newtonian case. Hofmann et al. (1997) [8] generalized the model of Qian & Woosley (1996) [5] and constrained the wind parameters. These investigations showed again that for the electron fractions and dynamical time scales reported by Woosley et al. (1994) [25], the entropy cannot reach values of $\sim 400 k_B/\text{nuc}$.

More advanced studies were performed by Otsuki et al. (2000) [6] and Thompson et al. (2001) [7]. These two detailed studies are independent of the supernova mechanism and thus provide general properties. They clearly demonstrated that general relativity increases the wind entropy (up to $\sim 40\%$) compared to Newtonian approach. Including such corrections in the neutrino treatment has a minor effect on the wind [6]: the bending of the neutrino trajectories increases the energy deposition (\dot{q}), while the redshift reduces it.

We use here Fig. 7 to illustrate which combination of wind parameters favour the r-process based on the steady-state models of Otsuki et al. (2000) [6]. Different neutron star masses (connected by solid lines) and various luminosities (connected by dashed lines) lead to different solutions in the entropy–time scale plane for $Y_e = 0.4$. The

color shadowed regions indicated the necessary conditions for the synthesis of elements up to the second and third r-process peak. Notice that this is possible only with very fast expansions (small dynamical time scale, $\tau_{\text{dyn}} < 0.03$ s) and high entropies ($S = 150 - 300 k_{\text{B}}/\text{nuc}$). This is achieved [6, 7] if the neutron star is very compact (i.e., a massive neutron star with small radius). Figure 7 clarifies the impact of the luminosity (Eqs. 7 and 8): lower luminosities lead to higher entropies but also slower expansion.

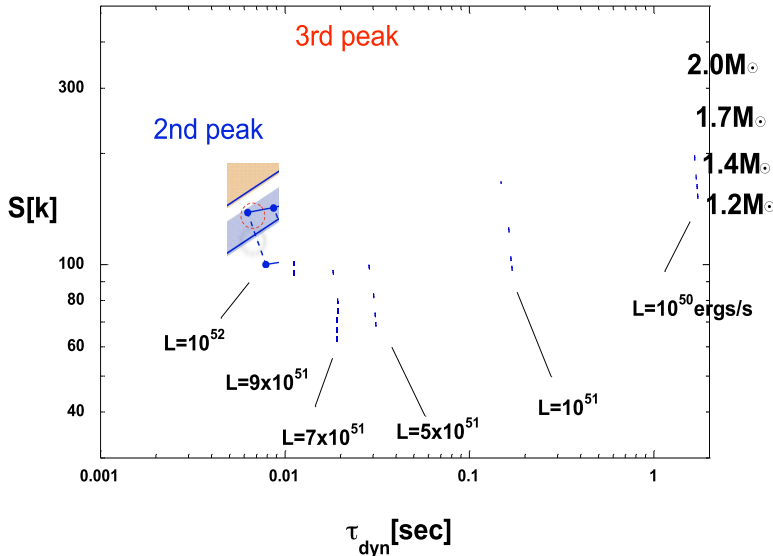


Figure 7. Figure courtesy of Kaori Otsuki. Every point corresponds to the solution of the steady wind equations [6] for given neutrino luminosities and neutron star masses as indicated in the figure. The electron fraction is $Y_e = 0.45$. The shadowed regions represent the necessary entropies and expansion time scales to obtain the second and third r-process peaks.

All these efforts, investigating the neutrino-driven winds with parametric models, did not lead to conditions which reproduce the r-process as reported in Woosley et al. (1994) [25]. Moreover, the first long-time hydrodynamic simulations [11], which could follow the wind during seconds with enough resolution, confirmed the results of steady state models even in two-dimensional models [41]. These simulations were performed with simplified neutrino transport, therefore the electron fraction obtained is not very exact. More sophisticated simulations using Boltzmann neutrino transport [13, 12] indicate that the neutrino-driven wind may be proton-rich in contrast to the very neutron-rich condition found by Woosley et al. (1994) [25]. Therefore, spherically symmetric neutrino-driven winds are not a reliable candidate to explain the origin of heavy elements via the r-process. However, the wind ejecta being slightly neutron rich or proton rich remain an exciting scenario for other nucleosynthesis processes (Sect. 3.2-3.4).

3.1.2. Impact of wind dynamical evolution on the r-process: If one assumes that the r-process occurs in high entropy neutrino-driven winds there are two important aspects that strongly affect the abundance of heavy elements: long-time dynamical evolution and nuclear physics input.

Most of the r-process studies in neutrino-driven winds have focused in finding the appropriated conditions to obtain a high neutron-to-seed ratio, which is determined in the early phase of the evolution during NSE and charged-particle reactions. However, the final r-process abundances (that one wants to compare to observation) are also affected by the long-time evolution when the temperature has already dropped to $T = 2 - 0.1$ GK. The wind termination has a strong impact on the evolution of the temperature at late times (Sect. 2.4). It was Wanajo (2007) [74] who defined two types of r-process depending on the dynamical evolution: a hot and a cold r-process. In the hot r-process the reverse shock is at relative high temperatures ($T \approx 1$ GK), there is an $(n, \gamma) - (\gamma, n)$ equilibrium and beta-decay time scales are longer than the neutron capture and photo-dissociation time scales. For the cold r-process, the photodissociation time scale becomes longer once the temperature drops below 0.5 G and the evolution proceeds by a competition between beta decay and neutron capture [75, 46].

The dependence of the abundances on the long-time evolution [47, 10, 45] is due to the different nuclear reactions that become important for every evolution. Therefore, the impact of the nuclear physics will also depend on the evolution as shown in detailed in Refs. [47, 10].

3.1.3. Impact of nuclear physics input on the r-process: In addition to the difficulties to find the astrophysical scenario where half of the heavy elements are produced in the universe [76, 77], only few of the very exotic nuclei involved in the r-process have been produced up to now in current rare isotope facilities [78]. Therefore, nucleosynthesis calculations rely on theoretical predictions towards extreme neutron-rich nuclei far from stability. There are several nuclear physics inputs with a strong impact on the final abundances.

Nuclear masses determine the energy thresholds for all relevant reactions: neutron capture, photodissociation, and beta decay. Their impact on the abundances have been studied (see e.g., [47, 10, 79, 80]) by using different theoretical mass models (e.g., FRDM [81], ETFSI [82], Dufflo & Zuker [83], HFB-x [84, 85]). Beta decay rates [86] control the speed of the r-process and during decay to stability become specially important due to the delayed neutron emission.

Reaction rates are also critical to understand the r-process. Neutron capture rates [87] have been shown to have a non-negligible impact on the final abundances as they shift the position of peaks and affect the rare-earth peak ($A \approx 160$) [88, 89, 47, 90]. Reactions involving neutrinos have been discussed extensively within the neutrino-driven wind models. Neutrino absorption on nuclei can mimic a beta decay and accelerates the r-process [91, 92], and also cause neutrino-induced neutron emission [93, 94] which can produce rare species from neighbouring nuclei with high abundances. While neutrino

absorption can speed up the r-process by mimicking β^- decays, it can also weaken an r-process by disintegrating alpha particles, which can then contribute to a larger seed nuclei population and thus a decreased neutron-to-seed ratio [95].

Fission can play an important role specially when several fission cycles occur [60, 96, 97, 98], leading to a robust r-process abundance pattern. The main fission channels include neutron induced fission, spontaneous fission, and beta-delayed fission [99, 100, 101, 97]. Neutrino-induced fission has been investigated in Ref. [102], but found to be negligible in neutrino-driven wind environments [103, 104].

A more detailed discussion of the impact of these nuclear physics inputs on the r-process is beyond the scope of this review.

3.2. Lighter heavy elements: Sr, Y, Zr

Although spherically symmetric neutrino-driven winds are not a good candidate for r-process, they are an exciting possibility to explain the origin of lighter heavy elements, such as Sr, Y, Zr. There are observational indications that several components or sites contribute to the so-called r-process elements. The r-process component results from subtracting the s-process component to the solar system abundances. The r-process is thus not consistently obtained by integrating the contribution of different sites within a galactic chemical evolution model. Therefore, the r-process component extracted from the solar system is not a real process but includes residual abundances left after removing the s-process. Moreover, observations of UMP stars [17] and meteorites [105] indicates that indeed several nucleosynthesis processes have contributed to build the abundances of the “residual r-process”.

The elemental abundances observed in the atmosphere of UMP stars [17, 106] present a robust pattern for heavy elements $56 < Z < 83$ in agreement with the solar r-process component. For few stars it has been possible to observe also Tellurium showing a robust pattern even for the second r-process peak [107]. In contrast, the abundances of lighter heavy elements $Z < 47$ show some scatter which points to the existence of at least two primary processes [17]. Observations suggest that there could be even three components or processes: 1) robust heavy r-process, 2) Sr, Y, Zr, 3) Ag and Pd [108].

The origin of lighter heavy elements (Sr, Y, Zr) was investigated by Travaglio et al (2004) [16] with their s-process calculation combined with a galactic chemical evolution model. The abundances of several isotopes (^{86}Sr , ^{93}Nb , ^{96}Mo , ^{100}Ru , ^{104}Pd , ^{110}Cd) could not be explained by adding s- and r-process (as observed in UMP stars) contributions. They suggested that these isotopes are produced by the Lighter Element Primary Process (LEPP), but they did not specify the astrophysical site nor the nuclear reactions involved. Other authors had proposed before that the process producing elements with $A < 130$ was a weak r-process [109] or charged-particle reactions [36, 9, 15]. Montes et al. (2007) [110] showed that there is an anticorrelation between heavy r-process and Sr-like elements in UMP stars. The elemental abundances of the Sr-like elements in UMP (stellar LEPP) agrees with the missing component in the solar system [16] (solar

LEPP), within the observational error bars (see abundances of HD 122563 in Fig. 5 of Ref. [110]). However, it remains an open question whether both are due to the same nucleosynthesis process.

Based on the observations of UMP stars, Qian and Wasserburg have developed a phenomenological model [111, 15, 66] to explain the astrophysical site and nucleosynthesis process contributing to the residual solar r-process abundances. In their model the lighter heavy elements are produced by charged-particle reactions in neutrino-driven winds. This has been confirmed [112] with hydrodynamical simulations of core-collapse supernovae and neutrino-driven winds using a parametrized electron fraction evolution. Roberts et al. (2010) [14] calculated also the integrated nucleosynthesis based on hydrodynamical simulations of the neutrino-driven wind. Figure 8 shows the elemental abundances based on neutrino-driven wind simulations and compared to observations. Note that different Y_e evolutions are employed to explore possible uncertainties in the neutrino physics. For neutron- and proton-rich conditions, LEPP elements are produced with different isotopic abundances. In neutron-rich winds, the composition is dominated by neutron-rich isotopes and there is even an overproduction for $A = 90$ (related to the magic number $N = 50$). In proton-rich winds the elemental-abundance pattern is quite robust against small variations of the wind parameters and the isotopic composition is characterized by neutron-deficient isotopes, i.e. those on the left side of stability. In the following sections we discuss the nucleosynthesis processes leading to these different isotopic abundances.

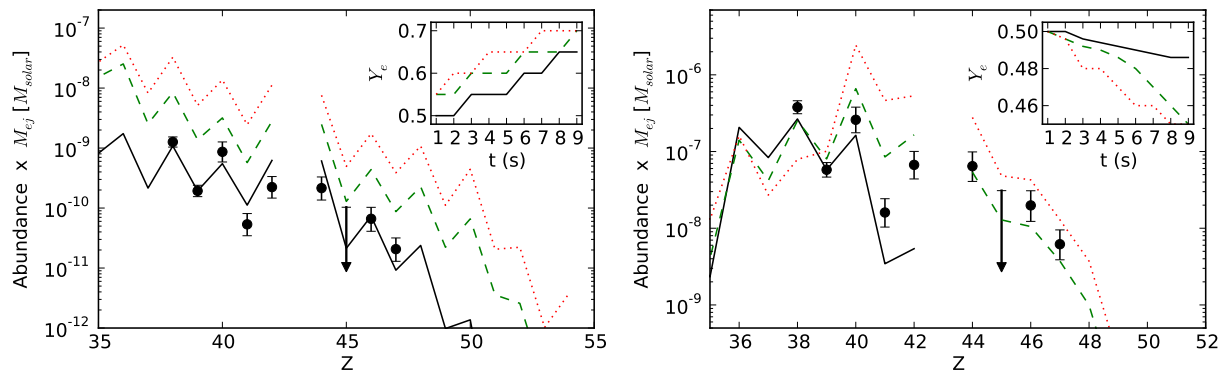


Figure 8. Elemental abundances for a superposition of mass zones with different electron fractions which are shown in the inset as a function of time after core collapse. The observed abundances [113, 114, 110] are shown by dots and rescaled to fit the solid line abundances.

3.3. Weak r-process

Most recent simulations predict proton-rich conditions, however there are still uncertainties on the neutrino physics which could lead to slightly neutron-rich conditions (Sect. 2.2, 2.4, [32, 33, 34]). Moreover, two-dimensional simulations of the explosion of

an ONeMg progenitor indicates that small neutron-rich pockets can be ejected because the expansion is very fast and neutrinos have not sufficient time to change their neutron richness [48]. Similar conditions are found in explosion based on an unrealistic quark phase transition [115].

The dependence of the weak r-process abundances on wind parameters have been investigated based on classical r-process models [116], which assume $(n, \gamma) - (\gamma, n)$ -equilibrium, and on dynamical parametric high entropy wind models [117]. These kind of studies aim to identify the astrophysical conditions which lead to good agreement between calculated and observed abundances. We have shown in Sect. 2.3 the composition of slightly neutron-rich wind based on the parametric wind trajectories presented in Appendix A. The abundance dependence on wind parameters (Fig. 4) can be understood by looking at the evolution of neutrons and seed nuclei in Fig. 3. There are several combinations of wind parameters (s, Y_e, τ) which produce the lighter heavy elements via a weak r-process and small variations of these parameters leads to different final abundances as shown in Ref. [112] for the LEPP.

The final abundances also depend on the long-time evolution which can be affected by the wind termination (see Appendix B for a simple parametrization). Figure 9 shows the density evolution and resulting abundances for different positions of the wind termination radius. Note that there is a shock, i.e. density jump, only when the wind is supersonic. The wind termination decelerates the expansion, allowing for further production of nuclei up to the iron group using alpha particles and neutrons. In the case without wind termination, the freeze-out of charged-particle reactions occurs faster and the Y_n/Y_{seed} is higher. This allows to build elements up to Sr, Y, Zr even when the entropy is low (upper panel). When the entropy is high, the wind termination has some impact on abundances only when it occurs at high temperatures. In this case, charged-particle reactions are effective during longer time, leading to higher abundances for $10 < Z < 40$. Independently of the wind termination position, the neutron magic number $N = 50$ is always reached and matter flow stops there.

Even more important than the reverse shock is the role of neutrinos. When neutrino luminosities are high and the wind is neutron-rich, electron neutrino absorption on neutrons lead to a significant reduction of the neutron-to-seed ratio. The impact of neutrinos on the weak r-process is presented in Fig. 10. When neutrinos are considered the production of lighter heavy elements is strongly hindered. High neutrino luminosities and energies may be found during the first second after the explosion. At later times the destruction of neutrons by neutrinos is less significant and lighter heavy elements are synthesized.

3.4. νp -process

Hydrodynamical simulations of core-collapse supernovae with sophisticated neutrino transport indicate that the early ejecta may be proton rich instead of neutron-rich [118, 119, 120, 121, 28, 122, 123]. Even long-time simulations suggest that spherically

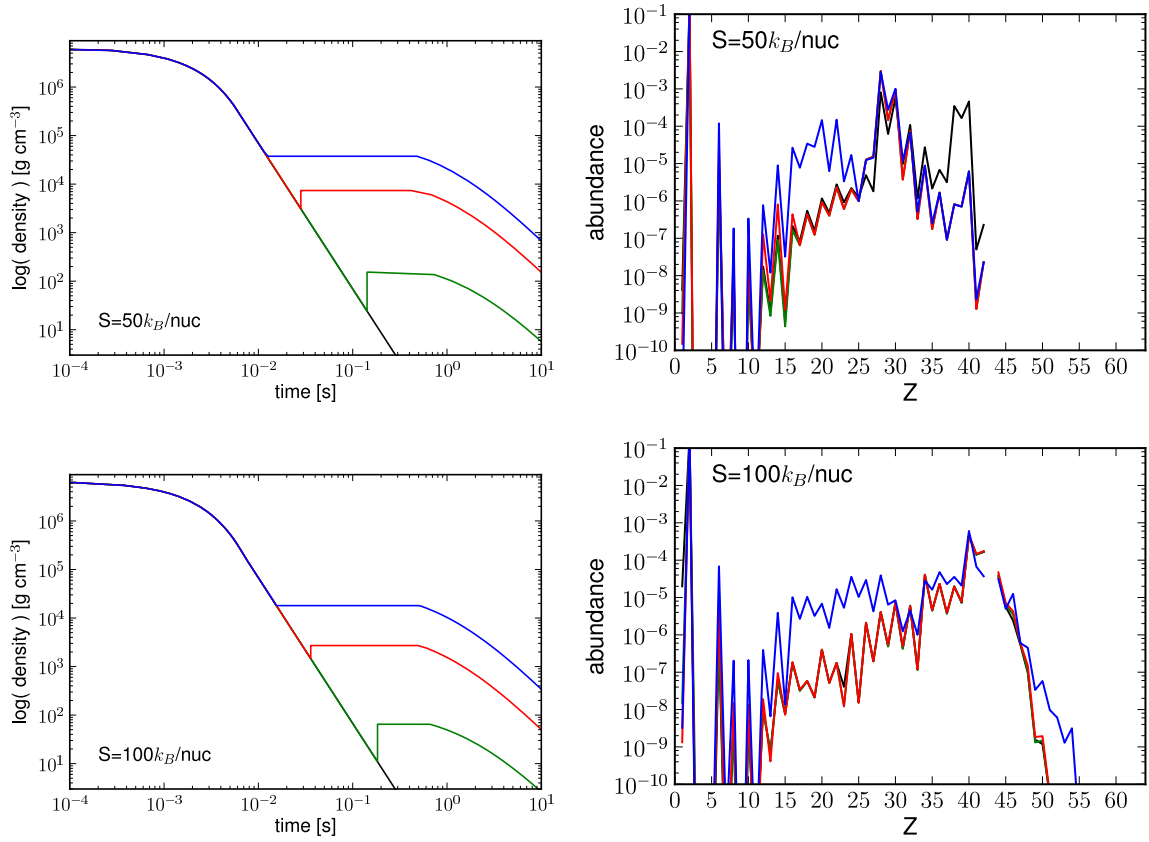


Figure 9. Left panels show the evolution of density assuming a wind termination at different positions. The expansion time scale is the same in both cases ($\tau = 2$ ms) and the entropy is indicated in the figures. The resulting elemental abundances are shown in the right column.

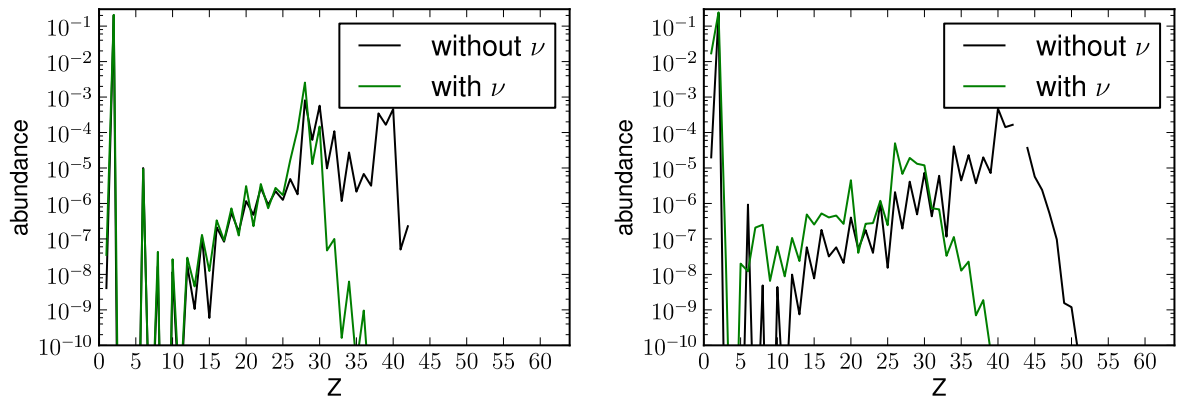


Figure 10. Elemental abundances with and without neutrinos for an expansion time scale of $\tau = 2$ ms and $Y_e = 0.49$. The entropy is $S = 50, 100 k_B/\text{nuc}$ in the left and right panels, respectively.

symmetric neutrino-driven winds could stay proton rich during several seconds [13, 12]. Although there are still uncertainties in the determination of the Y_e , it is very likely

that the neutrino-driven wind turns proton rich during some phase of the post explosion evolution.

In proton-rich condition elements beyond iron group can be synthesized by the νp -process [120, 28, 123]. Proton and alpha captures drive the matter flow up to ^{64}Ge which is a waiting point as its beta-decay half live is long compared to the expansion time scale of the wind. However, the matter is under a high neutrino flux and electron antineutrino absorption on protons produces a small amount of neutrons. These extra neutrons lead to (n, p) reactions which are faster than beta decays and thus permit the matter to flow towards heavier nuclei. The efficiency of this process strongly depends on the expansion time scale, entropy, electron fraction, but also on the neutrino luminosity and energies.

The most important role in the νp -process is played by neutrinos, or more specifically by electron antineutrinos. These are responsible to produce the necessary neutrons to overcome the bottlenecks. After the initial very fast expansion of a wind trajectory, there is an equilibrium between neutron capture and neutron production by antineutrino absorption on protons. This implies that

$$\frac{dY_n}{dt} = \lambda_{\bar{\nu}_e} Y_p - \sum_{Z,A} n_n Y(Z, A) \langle \sigma v \rangle_{(Z,A)} = 0. \quad (17)$$

Here $\lambda_{\bar{\nu}_e}$ is the electron antineutrino absorption rate and $\langle \sigma v \rangle_{(Z,A)}$ is the sum of reaction rates for (n, γ) and (n, p) reactions for nucleus (Z, A) . Therefore, the neutron density in equilibrium is given by

$$n_n = \frac{\lambda_{\bar{\nu}_e} Y_p}{\sum_{Z,A} Y(Z, A) \langle \sigma v \rangle_{(Z,A)}}. \quad (18)$$

The electron antineutrino luminosities and energies strongly determine the neutron density through $\lambda_{\bar{\nu}_e}$. Moreover, this equation shows clearly the importance of the proton-to-seed ratio for the νp -process.

The dependence of the abundances on the wind parameters for proton-rich condition is shown in Fig. 11. Similar to Fig. 4 we present results for different entropies in columns and various expansion time scales in rows. In addition, every panel contains the abundances for three electron fractions. The electron fraction affect the abundances as it determines proton abundances which are key for the production of neutrons as shown in Eq. (18). The other two wind parameters, i.e., entropy and expansion time scale, also influence the proton-to-seed and neutron-to-seed ratios and therefore the final abundances. As in neutron-rich conditions, high entropy prevents the formation of seed nuclei and this results in higher Y_p/Y_{seed} and Y_n/Y_{seed} . The impact of the expansion time scale follows also the same trend as in neutron-rich winds. The initial build up of the seed nuclei is controlled by three-body reactions which strongly depend on the expansion time scale (see Sect. 2.3). This is extreme for the very slow expansion, shown in the bottom panels of Fig. 11. Here all protons are consumed and final abundances are dominated by alpha particles and nuclei up to $Z = 40$. There are two peaks in the abundances related to the region around the waiting point ^{64}Ge and to $A \approx 90$ where

magic neutron number $N = 50$ and semi-magic proton number $Z = 40$ are reached. For faster expansions, the final abundances contain also protons because the temperature drops too fast without leaving enough time for the protons to be captured.

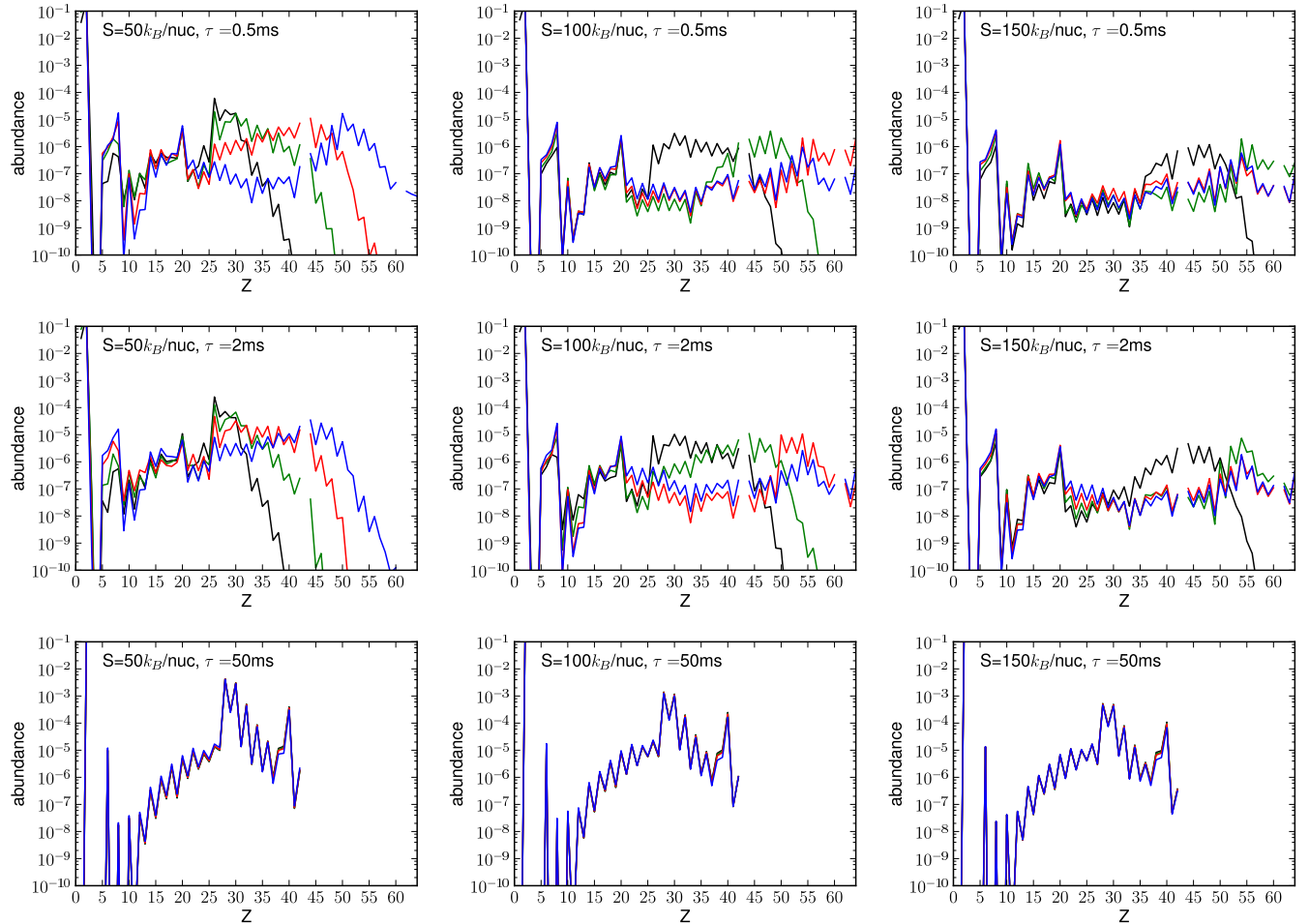


Figure 11. Elemental abundances for different electron fractions: $Y_e = 0.52$ (black), 0.55 (green), 0.60 (red), 0.65 (blue). The entropy and expansion time scale are given in the figures.

In order to understand the sensitivity of the abundances to neutrino luminosities and energies, we vary them for the wind with $Y_e = 0.52$, $S = 100 k_B/\text{nuc}$, and $\tau = 2$ ms. The resulting abundances are shown in Fig. 12. Without neutrinos the matter stays mainly in ^{56}Ni , which is the first bottleneck before ^{64}Ge . There is also a significant accumulation of matter between $Z = 26$ and $Z = 32$ in the cases with reduced neutrino luminosities and energies. However, the matter flow can continue toward heavier nuclei with the small amount of neutrons produced. When the neutrino luminosities or energies are increased by a factor two, the (n, p) reactions are more effective and heavier nuclei are produced.

In contrast to the weak r-process, where the reverse shock has a minor impact on the abundances, for the νp -process the wind termination can significantly modify the

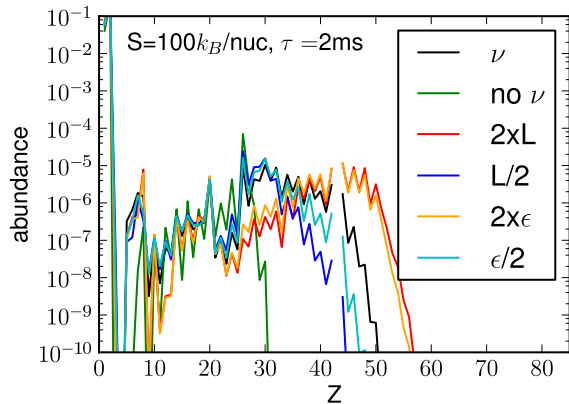


Figure 12. Elemental abundances with different neutrino treatment. The black line labeled as ν is the reference case and correspond to $Y_e = 0.52$, $S = 100 k_B/\text{nuc}$, and $\tau = 2$ ms (middle panel of Fig. 11). The other curves show calculations without neutrinos (no ν), with neutrino luminosities increased ($2\times L$) or decreased ($L/2$) by a factor of two, and with same variations for the neutrino energies.

abundances [124, 49]. The wind termination decelerates the expansion allowing the matter to stay under the antineutrino flux for longer time. Wanajo et al. (2011) [124] found that there is an optimal temperature for the wind termination around 2 GK to produce heavy elements. If the wind termination is much below this temperature, the expansion is too fast and antineutrinos have not sufficient time to produce the necessary neutrons to overcome bottlenecks. This kind of very fast expansion is usually found in low mass progenitors where there is not a termination shock and the νp -process is very inefficient [125, 126]. More massive progenitors lead to smaller wind termination radius and thus higher temperatures [11]. Very high temperature at the wind termination ($T \approx 3$ GK) hinder also the production of heavy elements, as matter stays in the newly identified ^{59}Cu (p, α) ^{56}Ni cycle [49]. When the wind termination is around 2 GK the charged-particle reactions are still very effective, a breakout from the NiCu-cycle can occur, and antineutrino still produce neutrons leading also to efficient (n, p) reactions. In addition to the temperature at the wind termination the evolution afterwards is also key to determine the abundances. This late evolution depends on the slow moving, early ejecta which are strongly affected by multi-dimensional anisotropies [41]. In some cases, the behaviour of density and temperature after the wind termination may lead to variations of the neutron density, allowing to move to stability not only by β -decay but also by neutron captures [41]. This is very important because it implies that matter can cross to the neutron-rich side of stability and even produce neutron-rich isotopes.

4. Summary and outlook

The present review discusses the mechanism of ejecting matter from the (proto-)neutron star surface via energy deposition of the neutrinos streaming out of the cooling

and deleptonizing neutron star after a successful supernova explosion (the so-called neutrino wind). The input physics entering this mechanism and its consequences for the composition of the ejected material are described in detail. The latter is strongly dependent on the neutron star nuclear equation of state, influencing the matter composition inside the neutron star, as well as the neutrino interactions with matter, both determining the final neutrino energy spectra and luminosities of all flavors.

While μ and τ -neutrinos are dominated by neutral current reactions, and pure scattering is not dominating the energy deposition nor changing the composition, electron neutrinos and anti-neutrinos act also via charged-current capture reactions (with strong energy deposition) which also determine the overall proton-to-nucleon ratio via $\nu_e + p \rightarrow n + e^+$ and $\bar{\nu}_e + n \rightarrow p + e^-$. Due to the energy dependence (and Q-values) of the neutrino and anti-neutrino cross sections, the composition becomes neutron-rich if average energies of anti-neutrinos are larger than those of neutrinos by $4 \times (m_n - m_p)c^2$, if both are characterized by similar total luminosities. More generally also the luminosities of both species enter.

Early calculations in the 90s resulted in substantial mean energy differences between anti-neutrinos and neutrinos, caused a neutron-rich composition and high entropies of the ejected matter. The entropy S , total proton-to-nucleon ratio Y_e , and the expansion time scale τ of ejected matter are the key properties for the composition of the ejecta (possibly still modified by late time behavior not corresponding to free expansions if matter experiences reverse shocks due to collision with matter ejected in the prior supernova explosion). These early calculations predicted a large neutron-to-seed ratio after freeze-out of charged particles reactions, providing the basis for a strong r-process and the production of heavy nuclei up to Th and U. This made the neutrino wind the most promising site for the r-process nuclei found in the solar composition and indicated a very strong production of r-process matter in the early Galaxy, as massive stars producing supernovae are the fastest evolving species and the earliest polluters of the interstellar medium (consistent with observations of low metallicity stars). These investigations also caused a large amount of parametrized calculations, studying r-process properties as a function of the three key parameters S , Y_e , and τ .

More recent core collapse simulations with late-time evolutions up to 10 s after core collapse, and improved micro physics and neutrino transport, resulted in anti-neutrino and neutrino spectra with smaller mean energy differences, and consequently a proton-rich composition of ejecta. This gave rise to a new process, the νp -process, where in a first step the more proton-rich conditions produce essential abundances of ^{64}Ge (decaying into ^{64}Zn , thus going beyond ^{56}Ni decaying into ^{56}Fe) which could explain that Zn is co-produced with Fe-group nuclei, as observed in low-metallicity stars. In a second step portions of ^{64}Ge can be processed further up to $A=90$ nuclei, due to overcoming its long beta-decay half-life via an (n, p) -reaction with neutrons, produced by anti-neutrino captures on the remaining free protons in this proton-rich environment. This opened an option to explain abundances of light p-nuclei.

Recent calculations, including medium effects for neutrons and protons, which lead

to effective Q-values corrected by chemical potential differences have apparently again provided a change. The full consequences of this effect are not fully analyzed, yet, and surprises are still expected. In any case, both proton-rich and slightly neutron-rich conditions are adequate to synthesized lighter heavy elements such as Sr, Y, Zr. Their abundances have been attributed before to a not-yet understood lighter (heavy) element primary process (LEPP) which is required in galactic evolution based on low-metallicity observations.

In addition, the final understanding will probably only arise with the full understanding of core collapse supernova explosions from 3D hydrodynamical modeling. The latter is well on its way, but not yet established. Thus, the neutrino wind properties will probably still provide further surprises and possibly even contain matter with properties covering all cases discussed above, due to the time evolution of neutrino spectra and luminosities.

Acknowledgments

A.A. was supported by a Feodor Lynen Fellowship (Humboldt Foundation) and by the Helmholtz-University Young Investigator grant No. VH-NG-825. F.K.T. acknowledge support by the Humboldt Research Award. We acknowledge support and funding by the Swiss National Science Foundation (SNF). The authors are additionally supported by EuroGENESIS, a collaborative research program of the European Science Foundation (ESF) and the Helmholtz Nuclear Astrophysics Virtual Institute (NAVI, VH-VI-417).

Appendix A. Parametric wind trajectories

We give an useful parametrization for wind trajectories based on hydrodynamical simulations. The evolution of density is assumed to be first exponential and then to follow a power law. The wind entropy is constant as the expansion is adiabatic. The reverse shock leads to an increase of density and entropy that will be also parametrized in the next section. Once density and entropy are known the temperature is obtained from an equation of state (see e.g., [37, 9]). The evolution of radius is provided by mass conservation in a steady state outflow: $\dot{M} = 4\pi r^2 v \rho = \text{constant}$ with $v = dr/dt$.

Here we assume the density drops exponentially between $T = 10$ GK and a lower limit temperature T_{exp} . This can be used as an additional parameter, although here we fix it to $T_{\text{exp}} = 4$ GK, i.e., the expansion is exponential while charged particle reactions dominate the evolution. Previous works assumed also a mixed evolution from exponential to power law (e.g., Ref. [127]) and they use an additional time scale to switch from one to the other.

For $T > T_{\text{exp}}$, density, radius, and velocity at a time $t > t_0$ (with t_0 being the initial time which fulfils $T(t_0) \approx 10$ GK) are given by:

$$\rho(t) = \rho_0 e^{(t_0-t)/\tau} \tag{A.1}$$

$$r(t) = r_0 \left[1 + 3 \frac{v_0}{r_0} \tau (e^{(t_0-t)/\tau} - 1) \right]^{1/3} \quad (\text{A.2})$$

$$v(t) = v_0 e^{(t_0-t)/\tau} \left[1 + 3 \frac{v_0}{r_0} \tau (e^{(t_0-t)/\tau} - 1) \right]^{-2/3} \quad (\text{A.3})$$

Here the quantities ρ_0 , r_0 , and v_0 correspond to density, radius, and velocity at the initial time t_0 , respectively. The expansion time scale is τ .

After the temperature drops below $T \sim T_{\text{exp}}$ the evolution continues as a power law:

$$\rho(t) = \rho_{\text{exp}} \left(\frac{t_{\text{exp}}}{t} \right)^3 \quad (\text{A.4})$$

$$r(t) = r_{\text{exp}} \left[1 + \frac{3 v_{\text{exp}} t_{\text{exp}}}{4 r_{\text{exp}}} \left(\left(\frac{t}{t_{\text{exp}}} \right)^4 - 1 \right) \right]^{1/3} \quad (\text{A.5})$$

$$v(t) = v_{\text{exp}} \left(\frac{t}{t_{\text{exp}}} \right)^3 \left[1 + \frac{3 v_{\text{exp}} t_{\text{exp}}}{4 r_{\text{exp}}} \left(\left(\frac{t}{t_{\text{exp}}} \right)^4 - 1 \right) \right]^{-2/3} \quad (\text{A.6})$$

The quantities ρ_{exp} , r_{exp} , v_{exp} , and t_{exp} correspond to the moment when the temperature is $T = T_{\text{exp}}$. Note that the velocity increases for $t \rightarrow \infty$, although in neutrino-driven winds the velocity asymptotically converges to a constant value. This can be cured by using a power law with $\rho \propto t^{-2}$ (see e.g., Ref.[46, 124] or by including the deceleration due to the interaction with the slow moving ejecta (see Appendix B).

Appendix B. Reverse shock

The main impact of the reverse shock on the evolution is the sudden deceleration of matter, which leads a drop of the expansion velocity and an increase of temperature and density, as kinetic energy is transformed into internal energy. This increase can be determined using the Rankine-Hugoniot conditions to calculate the values of the density (ρ_{rs}), temperature (T_{rs}), and velocity (u_{rs}) of the shocked material relative to the wind values (marked by the subscript “w”). The Rankine-Hugoniot conditions for mass, momentum, and energy conservation through the shock and are given by:

$$\rho_w u_w = \rho_{\text{rs}} u_{\text{rs}} \quad (\text{B.1})$$

$$P_w + \rho_w u_w^2 = P_{\text{rs}} + \rho_{\text{rs}} u_{\text{rs}}^2 \quad (\text{B.2})$$

$$\frac{1}{2} u_w^2 + \epsilon_w + \frac{P_w}{\rho_w} = \frac{1}{2} u_{\text{rs}}^2 + \epsilon_{\text{rs}} + \frac{P_{\text{rs}}}{\rho_{\text{rs}}} \quad (\text{B.3})$$

here ρ , v , P , and ϵ are the density, velocity, pressure, and specific internal energy, respectively. In the last equation one can take $\epsilon \approx 3P/\rho$ because it is radiation dominated environment. Assuming that the lhs of these equations is known, thus combining the three equations one gets two possible solutions for the matter velocity after the shock: 1) $u_{\text{rs}} = u_w$, no shock; 2) $u_{\text{rs}} = u_w/7 + 8/7 P_w/(\rho_w u_w)$. Once the velocity is known, the density and pressure can be computed using Eqs. (B.1), (B.2).

The evolution of density after the reverse shock can be determined from the condition of constant mass outflow: $\dot{M} = 4\pi r^2 v \rho$. There are two extreme possibilities: 1) velocity is constant and density decreases as r^{-2} ; 2) density is constant and therefore velocity drops as r^{-2} . The latter was used in Ref. [45]. However, it implies a decrease of the velocity down to a few m s^{-1} in about a second, that is not consistent with simulations [11, 12], where the post-shock velocities are around 10^3 – 10^4 km s^{-1} . The simulations suggest something in between these two extremes. First the density stays almost constant during $\approx 0.5 - 1 \text{ s}$ and the velocity decreases as r^{-2} , later the velocity stays constant and consequently the density decreases as r^{-2} . Once the density is known the temperature can be determined from the condition of constant entropy (adiabatic expansion).

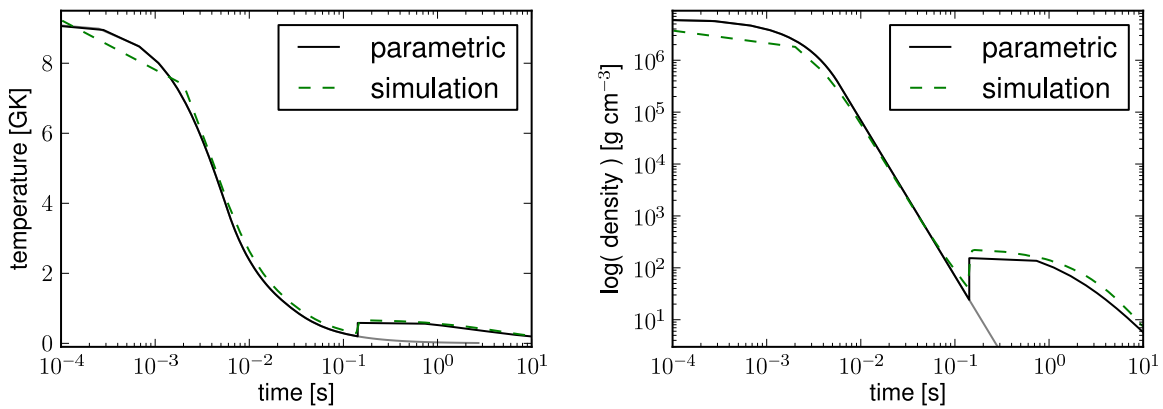


Figure B1. Comparison of temperature and density evolutions from the supernova simulation (trajectory ejected 5 s after bounce of model M1511r1 of Ref. [11]) to the evolution based on our parametric description. The grey solid line corresponds to the evolution without wind termination (Appendix A).

A comparison between the parametric expansion and the results from the simulations is presented in Figure B1. The grey line corresponds to the expansion without reverse shock as introduced in Appendix A. The dashed green line from the simulation has lower resolution than the parametrization. This explains the initial differences.

References

- [1] E. M. Burbidge, G. R. Burbidge, W. A. Fowler, and F. Hoyle. *Rev. Mod. Phys.*, 29, 547, 1957.
- [2] A. G. W. Cameron. *pasp*, 69, 201, June 1957.
- [3] H.-T. Janka, K. Langanke, A. Marek, G. Martínez-Pinedo, and B. Müller. *Phys. Rep.*, 442, 38, April 2007.
- [4] H.-T. Janka. *arXiv:1206.2503*, 2012.
- [5] Y.-Z. Qian and S. E. Woosley. *ApJ*, 471, 331, 1996.
- [6] K. Otsuki, H. Tagoshi, T. Kajino, and S. Wanajo. *ApJ*, 533, 424, 2000.
- [7] T A. Thompson, A. Burrows, and B. S. Meyer. *ApJ*, 562, 887, 2001.
- [8] R. D. Hoffman, S. E. Woosley, and Y.-Z. Qian. *ApJ*, 482, 951, 1997.

- [9] C. Freiburghaus, J.-F. Rembges, T. Rauscher, E. Kolbe, F.-K. Thielemann, K.-L. Kratz, B. Pfeiffer, and J. J. Cowan. *ApJ*, 516, 381, 1999.
- [10] K. Farouqi, K.-L. Kratz, B. Pfeiffer, T. Rauscher, F.-K. Thielemann, and J. W. Truran. *ApJ*, 712, 1359, 2010.
- [11] A. Arcones, H.-T. Janka, and L. Scheck. *A&A*, 467, 1227, 2007.
- [12] T. Fischer, S. C. Whitehouse, A. Mezzacappa, F.-K. Thielemann, and M. Liebendörfer. *A&A*, 517, A80, 2010.
- [13] L. Hüdepohl, B. Müller, H.-T. Janka, A. Marek, and G. G. Raffelt. *Phys. Rev. Lett.*, 104, 251101, 2010.
- [14] L. F. Roberts, S. E. Woosley, and R. D. Hoffman. *ApJ*, 722, 954, 2010.
- [15] Y.-Z. Qian and G. J. Wasserburg. *Phys. Rep.*, 442, 237, 2007.
- [16] C. Travaglio, R. Gallino, E. Arnone, J. Cowan, F. Jordan, and C. Sneden. *ApJ*, 601, 864, 2004.
aaaa
- [17] C. Sneden, J. J. Cowan, and R. Gallino. *Ann. Rev. Astron. & Astrophys.*, 46,241, 2008.
- [18] P. S. Barklem, N. Christlieb, T. C. Beers, V. Hill, M. S. Bessell, J. Holmberg, B. Marsteller, S. Rossi, F.-J. Zickgraf, and D. Reimers. *A&A*, 439, 129, 2005.
- [19] H. Aihara and et al. *ApJS*, 193, 29, 2011.
- [20] J. J. Cowan and F.-K. Thielemann. *Physics Today*, 57(10):100000, 2004.
- [21] W. R. Hix and F.-K. Thielemann. *Journal of Computational and Applied Mathematics*, 109, 321, 1999.
- [22] R. C. Duncan, S. L. Shapiro, and I. Wasserman. *ApJ*, 309, 141, 1986.
- [23] J. A. Pons, S. Reddy, M. Prakash, J. M. Lattimer, and J. A. Miralles. *ApJ*, 513, 780, 1999.
- [24] H.-T. Janka. *A&A*, 368, 527, 2001.
- [25] S. E. Woosley, J. R. Wilson, G. J. Mathews, R. D. Hoffman, and B. S. Meyer. *ApJ*, 433, 229, 1994.
- [26] B. S. Meyer, G. J. Mathews, W. M. Howard, S. E. Woosley, and R. D. Hoffman. *ApJ*, 399, 656, 1992.
- [27] B. S. Meyer. Entropy and nucleosynthesis. *Phys. Rep.*, 227, 257, 1993.
- [28] C. Fröhlich, G. Martínez-Pinedo, M. Liebendörfer, F.-K. Thielemann, E. Bravo, W. R. Hix, K. Langanke, and N. T. Zinner. *Phys. Rev. Lett.*, 96, 142502, 2006.
- [29] A. Arcones, G. Martínez-Pinedo, E. O'Connor, A. Schwenk, H.-T. Janka, C. J. Horowitz, and K. Langanke. *Phys. Rev. C*, 78, 015806, 2008.
- [30] T. Fischer, G. Martínez-Pinedo, M. Hempel, and M. Liebendörfer. *Phys. Rev. D*, 85, 083003, 2012.
- [31] S. Bacca, K. Hally, M. Liebendörfer, A. Perego, C. J. Pethick, and A. Schwenk. *arXiv:1112.5185*, 2011.
- [32] G. Martínez-Pinedo, T. Fischer, A. Lohs, and L. Huther. *arXiv:1205.2793*, 2012.
- [33] L. F. Roberts. *arXiv:1205.3228*, 2012.
- [34] L. F. Roberts and S. Reddy. Medium modification of the charged current neutrino opacity and its implications. *arXiv:1205.4066*, 2012.
- [35] Sanjay Reddy, Madappa Prakash, and James M. Lattimer. *Phys. Rev. D*, 58, 013009, 1998.
- [36] S. E. Woosley and R. D. Hoffman. *ApJ*, 395, 202, 1992.
- [37] J. Wittl, H.-T. Janka, and K. Takahashi. *A&A*, 286, 841, 1994.
- [38] H.-T. Janka and E. Müller. *ApJL*, 448, L109, 1995.
- [39] H.-T. Janka and E. Müller. *A&A*, 306, 167, 1996.
- [40] A. Burrows, J. Hayes, and B. A. Fryxell. *ApJ*, 450, 830, 1995.
- [41] A. Arcones and H.-T. Janka. *A&A*, 526, A160, 2011.
- [42] S. Wanajo, T. Kajino, G. J. Mathews, and K. Otsuki. *ApJ*, 554, 578, 2001.
- [43] M. Terasawa, K. Sumiyoshi, S. Yamada, H. Suzuki, and T. Kajino. *ApJ*, 578, L137, 2002.
- [44] S. Wanajo, N. Itoh, Y. Ishimaru, S. Nozawa, and T. C. Beers. *ApJ*, 577, 853, 2002.
- [45] T. Kuroda, S. Wanajo, and K. Nomoto. *ApJ*, 672, 1068, 2008.

- [46] I. V. Panov and H.-T. Janka. *A&A*, 494, 829, 2009.
- [47] A. Arcones and G. Martínez-Pinedo. *Phys. Rev. C*, 83, 045809, 2011.
- [48] S. Wanajo, H.-T. Janka, and B. Müller. *ApJL*, 726, L15, 2011.
- [49] A. Arcones, C. Fröhlich, and G. Martínez-Pinedo. *ApJ*, 750, 18, 2012.
- [50] S. Wanajo. *ApJL*, 650, L79, 2006.
- [51] S. Nagataki and K. Kohri. *PASJ*, 53:547–553, June 2001.
- [52] T. A. Thompson. *ApJL*, 585, L33, 2003.
- [53] T. K. Suzuki and S. Nagataki. *ApJ*, 628, 914, 2005.
- [54] B. D. Metzger, T. A. Thompson, and E. Quataert. *ApJ*, 659, 561, 2007.
- [55] C. Thompson and R. C. Duncan. *ApJ*, 408, 194, 1993.
- [56] H. Duan, G. M. Fuller, and Y.-Z. Qian. *Annual Review of Nuclear and Particle Science*, 60, 569, 2010.
- [57] G. Martínez-Pinedo, B. Ziebarth, T. Fischer, and K. Langanke. *European Physical Journal A*, 47, 98, 2011.
- [58] G. C. McLaughlin, J. M. Fetter, A. B. Balantekin, and G. M. Fuller. *Phys. Rev. C*, 59, 2873, 1999.
- [59] K. N. Abazajian et al. *arXiv:1204.5379*, April 2012.
- [60] J. Beun, G. C. McLaughlin, R. Surman, and W. R. Hix. *Phys. Rev. D*, 73, 093007, 2006.
- [61] J. Fetter, G. C. McLaughlin, A. B. Balantekin, and G. M. Fuller. *Astroparticle Physics*, 18, 433, 2003.
- [62] J. Hidaka and G. M. Fuller. *Phys. Rev. D*, 76, 083516, 2007.
- [63] I. Tamborra, G. G. Raffelt, L. Hüdepohl, and H.-T. Janka. *Journal of Cosmology and Astroparticle Physics*, 1, 13, 2012.
- [64] W. Hillebrandt, T. Kodama, and K. Takahashi. *A&A*, 52, 63, 1976.
- [65] G. J. Mathews and J. J. Cowan. *Nature*, 345, 491, 1990.
- [66] Y.-Z. Qian and G. J. Wasserburg. *ApJ*, 687, 272, 2008.
- [67] E. S. Myra and S. A. Bludman. *ApJ*, 340, 384, 1989.
- [68] H. A. Bethe. *Reviews of Modern Physics*, 62, 801, 1990.
- [69] F. S. Kitaura, H.-T. Janka, and W. Hillebrandt. *A&A*, 450, 345, 2006.
- [70] H. A. Bethe and J. R. Wilson. *ApJ*, 295, 14, 1985.
- [71] J. R. Wilson and R. W. Mayle. *Phys. Rep.*, 227, 97, 1993.
- [72] K. Takahashi, J. Wittl, and H.-T. Janka. *A&A*, 286, 857, 1994.
- [73] C. Y. Cardall and G. M. Fuller. *ApJL*, 486, L111, 1997.
- [74] S. Wanajo. *ApJL*, 666, L77, 2007.
- [75] J. B. Blake and D. N. Schramm. *ApJ*, 209, 846, 1976.
- [76] F.-K. Thielemann, A. Arcones, R. Käppeli, M. Liebendörfer, T. Rauscher, C. Winteler, C. Fröhlich, I. Dillmann, T. Fischer, G. Martínez-Pinedo, K. Langanke, K. Farouqi, K.-L. Kratz, I. Panov, and I. K. Korneev. *Progress in Particle and Nuclear Physics*, 66, 346, 2011.
- [77] M. Arnould, S. Goriely, and K. Takahashi. *Phys. Repts.*, 450, 97, 2007.
- [78] K.-L. Kratz, K. Farouqi, and B. Pfeiffer. *Progress in Particle and Nuclear Physics*, 59, 147, 2007.
- [79] K. Kratz, J. Bitouzet, F. Thielemann, P. Moeller, and B. Pfeiffer. *ApJ*, 403, 216, 1993.
- [80] A. Arcones and G. F. Bertsch. *Phys. Rev. Lett.*, 108, 151101, 2012.
- [81] P. Möller, J. R. Nix, W. D. Myers, and W. J. Swiatecki. *Atomic Data and Nuclear Data Tables*, 59,185, 1995.
- [82] Y. Aboussir, J. M. Pearson, A. K. Dutta, and F. Tondeur. *Atomic Data and Nuclear Data Tables*, 61,127, 1995.
- [83] J. Duflo and A. P. Zuker. *Phys. Rev. C*, 52, 23, 1995.
- [84] S. Goriely, N. Chamel, and J. M. Pearson. *Phys. Rev. Lett.*, 102, 152503, 2009.
- [85] S. Goriely, N. Chamel, and J. M. Pearson. *Phys. Rev. C*, 82, 035804, 2010.
- [86] P. Möller, B. Pfeiffer, and K.-L. Kratz. *Phys. Rev. C*, 67, 055802, 2003.
- [87] T. Rauscher and F.-K. Thielemann. *Atomic Data and Nuclear Data Tables*, 88, 1, 2004.

- [88] R. Surman, J. Engel, J. R. Bennett, and B. S. Meyer. *Phys. Rev. Lett.*, 79, 1809, 1997.
- [89] R. Surman, J. Beun, G. C. McLaughlin, and W. R. Hix. *Phys. Rev. C*, 79, 45809, 2009.
- [90] M. R. Mumpower, G. C. McLaughlin, and R. Surman. *Phys. Rev. C*, 85, 045801, 2012.
- [91] G. M. Fuller and B. S. Meyer. *ApJ*, 453, 792, 1995.
- [92] G. C. McLaughlin, G. M. Fuller, and J. R. Wilson. *ApJ*, 472, 440, 1996.
- [93] Y.-Z. Qian, W. C. Haxton, K. Langanke, and P. Vogel. *Phys. Rev. C*, 55, 1532, 1997.
- [94] W. C. Haxton, K. Langanke, Y.-Z. Qian, and P. Vogel. *Phys. Rev. Lett.*, 78, 2694, 1997.
- [95] B. S. Meyer. *ApJL*, 449, L55, 1995.
- [96] J. Beun, G. C. McLaughlin, R. Surman, and W. R. Hix. *Phys. Rev. C*, 77, 035804, 2008.
- [97] I. V. Panov, E. Kolbe, B. Pfeiffer, T. Rauscher, K.-L. Kratz, and F.-K. Thielemann. *Nuclear Physics A*, 747, 633, 2005.
- [98] I. V. Panov, I. Y. Korneev, T. Rauscher, G. Martínez-Pinedo, A. Kelić-Heil, N. T. Zinner, and F.-K. Thielemann. *Astron. & Astrophys.*, 513, A61, 2010.
- [99] A. Mamdouh, J. M. Pearson, M. Rayet, and F. Tondeur. *Nuclear Physics A*, 644, 389, 1998.
- [100] W. D. Myers and W. J. Świątecki. *Phys. Rev. C*, 60, 014606, 1999.
- [101] S. Goriely, S. Hilaire, A. J. Koning, M. Sin, and R. Capote. *Phys. Rev. C*, 79, 024612, 2009.
- [102] E. Kolbe, K. Langanke, and G. M. Fuller. *Phys. Rev. Lett.*, 92, 111101, 2004.
- [103] F.-K. Thielemann, D. Mocerlj, I. Panov, E. Kolbe, T. Rauscher, K.-L. Kratz, K. Farouqi, B. Pfeiffer, G. Martinez-Pinedo, A. Kelic, K. Langanke, K.-H. Schmidt, and N. Zinner. *International Journal of Modern Physics E*, 16, 1149, 2007.
- [104] G. Martínez-Pinedo, D. Mocerlj, N.T. Zinner, A. Kelić, K. Langanke, I. Panov, B. Pfeiffer, T. Rauscher, K.-H. Schmidt, and F.-K. Thielemann. *Progress in Particle and Nuclear Physics*, 59(1), 199, 2007.
- [105] G. J. Wasserburg, M. Busso, and R. Gallino. *ApJL*, 466, L109, 1996.
- [106] J. A. Johnson and M. Bolte. *ApJ*, 579, 616, 2002.
- [107] I. U. Roederer, J. E. Lawler, J. J. Cowan, T. C. Beers, A. Frebel, I. I. Ivans, H. Schatz, J. S. Sobek, and C. Sneden. *ApJL*, 747, L8, 2012.
- [108] C. J. Hansen and F. Primas. *A&A*, 525, L5, 2011.
- [109] J. W. Truran and J. J. Cowan. In W. Hillebrandt & E. Müller, editor, *Nuclear Astrophysics, 2000*, 64, 2000.
- [110] F. Montes, T. C. Beers, J. Cowan, T. Elliot, K. Farouqi, R. Gallino, M. Heil, K.-L. Kratz, B. Pfeiffer, M. Pignatari, and H. Schatz. *ApJ*, 671, 1685, 2007.
- [111] Y.-Z. Qian and G. J. Wasserburg. *ApJ*, 559, 925, 2001.
- [112] A. Arcones and F. Montes. *ApJ*, 731, 5, 2011.
- [113] S. Honda, W. Aoki, T. Kajino, H. Ando, T. C. Beers, H. Izumiura, K. Sadakane, and M. Takada-Hidai. *ApJ*, 607, 474, 2004.
- [114] S. Honda, W. Aoki, Y. Ishimaru, S. Wanajo, and S. G. Ryan. *ApJ*, 643, 1180, 2006.
- [115] N. Nishimura, T. Fischer, F.-K. Thielemann, C. Fröhlich, M. Hempel, R. Käppeli, G. Martínez-Pinedo, T. Rauscher, I. Sagert, and C. Winteler. *arXiv:1112.5684*, 2011.
- [116] K.-L. Kratz, K. Farouqi, B. Pfeiffer, J. W. Truran, C. Sneden, and J. J. Cowan. *ApJ*, 662, 39, 2007.
- [117] K. Farouqi, K.-L. Kratz, L. I. Mashonkina, B. Pfeiffer, J. J. Cowan, F.-K. Thielemann, and J. W. Truran. *ApJL*, 694, L49, 2009.
- [118] M. Liebendörfer, A. Mezzacappa, O. E. B. Messer, G. Martinez-Pinedo, W. R. Hix, and F.-K. Thielemann. *Nuclear Physics A*, 719, 144, 2003.
- [119] J. Pruet, S. E. Woosley, R. Buras, H.-T. Janka, and R. D. Hoffman. *ApJ*, 623, 325, 2005.
- [120] J. Pruet, R. D. Hoffman, S. E. Woosley, H.-T. Janka, and R. Buras. *ApJ*, 644, 1028, 2006.
- [121] C. Fröhlich, P. Hauser, M. Liebendörfer, G. Martínez-Pinedo, F.-K. Thielemann, E. Bravo, N. T. Zinner, W. R. Hix, K. Langanke, A. Mezzacappa, and K. Nomoto. *ApJ*, 637, 415, 2006.
- [122] R. Buras, M. Rampp, H.-T. Janka, and K. Kifonidis. *A&A*, 447, 1049, 2006.
- [123] S. Wanajo. *ApJ*, 647, 1323, 2006.

- [124] S. Wanajo, H.-T. Janka, and S. Kubono. *ApJ*, 729, 46, 2011.
- [125] S. Wanajo, K. Nomoto, H.-T. Janka, F. S. Kitaura, and B. Müller. *ApJ*, 695, 208, 2009.
- [126] R. D. Hoffman, B. Müller, and H.-T. Janka. *ApJL*, 676, L127, 2008.
- [127] B. S. Meyer. *Phys. Rev. Lett.*, 89, 231101, 2002.